EXPERIMENT AND MODELING OF COPPER INDIUM GALLIUM DISELENIDE (CIGS) SOLAR CELL: EFFECT OF AXIAL LOADING AND ROLLING

by
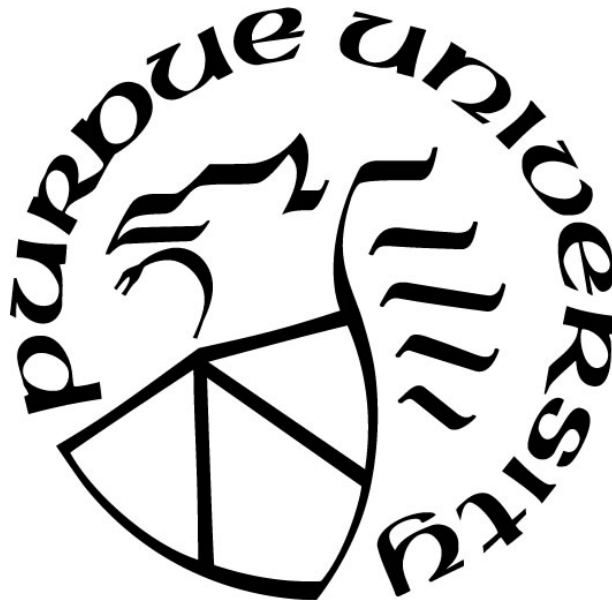
Arturo S. Garcia

A Thesis

Submitted to the Faculty of Purdue University
In Partial Fulfillment of the Requirements for the degree of

Master of Science in Mechanical Engineering

Department of Mechanical and Civil Engineering

Hammond, Indiana

May 2020

THE PURDUE UNIVERSITY GRADUATE SCHOOL
STATEMENT OF COMMITTEE APPROVAL

Dr. Hansung Kim, Chair

Department of Mechanical and Civil Engineering

Dr. Xiuling Wang

Department of Mechanical and Civil Engineering

Dr. Nesrin Ozalp

Department of Mechanical and Civil Engineering

Approved by:

Dr. Chenn Zhou

To my family, Mother, two sisters, two brothers, and especially my father thank you all for your support.

ACKNOWLEDGMENTS

TABLE OF CONTENTS

LIST OF TABLES

LIST OF FIGURES

LIST OF SYMBOLS

J-V	Current density versus voltage
V_{oc}	Open-circuit voltage
J_{sc}	Short-circuit current density
FF	Fill factor
EFF, η	Efficiency
V_{mp}	Voltage at maximum power point
J_{mp}	Current density at maximum power point
P_{max}	Maximum power
P_0	Input power
$\emptyset$	Electrostatic potential
U_n	Recombination rate for electron
U_p	Recombination rate for hole
G_n	Generation rate for electro
G_p	Generation rate for hole
ρ	Charge concentration
J_n	Electron current density
J_p	Hole current density
n	Electron concentration
p	Hole concentration
EM, μ_n	Electron mobility
HM, μ_p	Hole mobility
D_n	Diffusion coefficient of electron
D_p	Diffusion coefficient of hole
μ	Carrier mobility
k_B	Boltzmann constant

E_g	Band gap
E_c	Conduction band edge
E_v	Valence band edge
N_c	Effective density of state of conduction bands
N_V	Effective density of state of valance bands
m_e^*	Effective mass of electron
m_h^*	Effective mass of hole
h	Planck constant
x	Electron affinity
v_{th}	Thermal velocity
E_t	Trap energy level
n_i	Intrinsic carrier concentration
EL,HL, $\tau_{n,p}$	Electron and hole lifetime
$\sigma_{n,p}$	Electron and hole capture cross sections
N_t	Trap concentration
β	Stress
F	Force
γ	strain
∇l	Change in length
l_0	Initial length
S	intensity
S_0	Point source
S_n	Intensity normal to a surface
d	Distance from light source to any point on a cell
a_0	Fixed distance of the light source from the origin

R	Distance of the light source to the cell in the xy-plane
ω	Angle between the oncoming light ray and the normal to the cell face in the xy-plane-
ω_2	Angle between the tangents lines in the z axis and the oncoming light ray
m_1	The inverse slope of the incoming light ray
m_2	The inverse slope of the normal to the cell face.
r_c	The radius of cell curvature
K	The cell's centroid off set along the y- axis
D	The depth of the arc made by a curved cell
W	Width of the arc made by a curved cell
λ	wavelength
$EQE(\lambda)$	External Quantum Efficiency at a given wavelength
$EQE^{Ref}(\lambda)$	Reference External Quantum Efficiency at a given wavelength
I_L^{Ref}	Reference photo-generated current at given wavelength
I_L	Photo-generated current
I_0	Saturation current or dark current
R_S	Series resistance
R_{Sh}	Shunt Resistance
E	General energy
f	Frequency

ABSTRACT

In this paper various applications of axial tensile load, bending load, and rolling loading has been applied to a Copper Indium Gallium Diselenide (CIGS) Solar Cell to lean how it would affect the solar cell parameters of: Open circuit voltage (V_{oc}), Short circuit current, (I_{sc}), Maximum power (P_{max}), and Efficiency (EFF), and Fill Factor (FF). These Relationships were found for with three different experiments.

The first experiment the applies axial tensile stress is to a CIGS solar cell ranging from 0 to 200 psi with various strain rates: 0.0001, 0.001, 0.01, and 0.1 in/sec as well as various relaxation time: 1min, 5min, and 10 min while the performance of solar cell is measured. The results of this gave several trends couple pertaining the V_{oc} . The first is that open circuit voltage increases slightly with increasing stress. The second is the rate of increase (the slope) increases with longer relaxation times. The second set of trend pertains to the I_{sc}. The first is that short circuit current generally is larger with larger stress. The second is there seems to be a general increase in the Isc up to a given threshold of stress. After that threshold the Isc seems to decrease. The threshold stress varies depending on strain rate and relaxation time.

The second set of experiments consisted of holding a CIGS solar cell in a fixed curved position while it was in operational use. The radii of the curved cells were: 0.41, 0.20, 0.16, 0.13, 0.11, 0.094, and 0.082 m. The radii were performed for both concave and convex cell curvature. The trends for this show a slight decrease in all cell parameters with decreasing radii, the exception being V_{oc} which is not effecting, the convex curvature causing a slightly faster decrease than the concave. This set of experiments were also processed to find the trends of the single diode model parameters of series resistance (R_s), shunt resistance (R_{sh}), dark current (I_0), and saturation current (IL), which agreed with the experimental results.

The second experiment consisted of rolling a CIGS solar cell in tensile (cells towards dowel.) and compression (cells away from dowel) around a dowel to create internal damage. The diameter of the dowels decreased. The dowel diameters were: 2. 1.75, 1.25, 1, 0.75, 0.5, and 0.25 inches. This experiment showed similar trends as the bending one but also had a critical diameter of 1.75 in where beyond that damage much greater.

Finally a parametric study was done in COMSOL Multiphysics® to examine how changes in the CIGS material properties of electron mobility (EM), electron life time, (EL), hole mobility

(HM), and Hole life time (HL) effect the cell parameters. The trends are of an exponential manner that converges to a given value as the material properties increase. When EL, EM, HL are very small, on the order of 10^{-4} times smaller than their accepted values, a transient like responses occurs.

.

1. INTRODUCTION

1.1 Current Energy Situation

Mankind is greedy. It takes and consumes all the world has to offer and then some. Humans do this to sustain their ever growing needs and desires. Yet mankind hardly ever gives anything back to the earth and only demands more from it. This constant take is true for the world's energy consumption too. The International Energy Outlook 2019 [1] (IEO) makes clear how greedy mankind is and how bad they well get in their consumption of energy.

Figure 1 shows the world's total past and projected energy consumption for both countries that part of the Organization of Economic Cooperation and Development (OECD) and countries not associated with the OECD since their economic development and energy consumption differ. It is clear that over the next fifty years the world energy consumption would increase by a factor of 1.5.
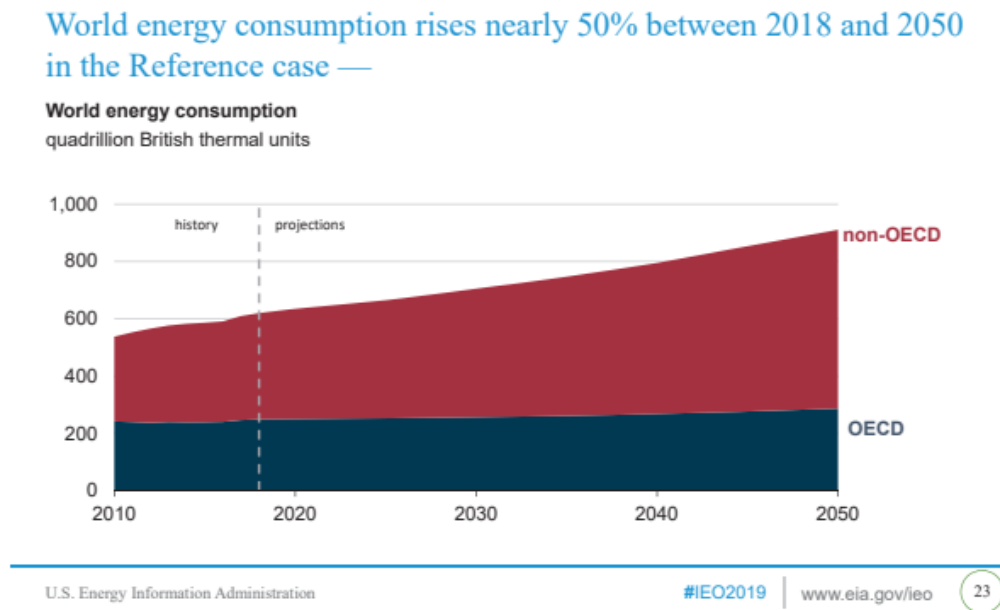
Figure 1: Past world energy consumption and world energy consumption projections out to 2050[1]

With this glaring need for more energy and the current progression of environmental damage it has created, man was prompted to seek out methods of production which do not take

16

so as much from the planet. As the IEO shows in figure 2 the production of renewable energies greatly increases

Renewable energy becomes the leading source of primary energy consumption by 2050 in the Reference case—

Primary energy consumption by energy source, world
quadrillion British thermal units

share
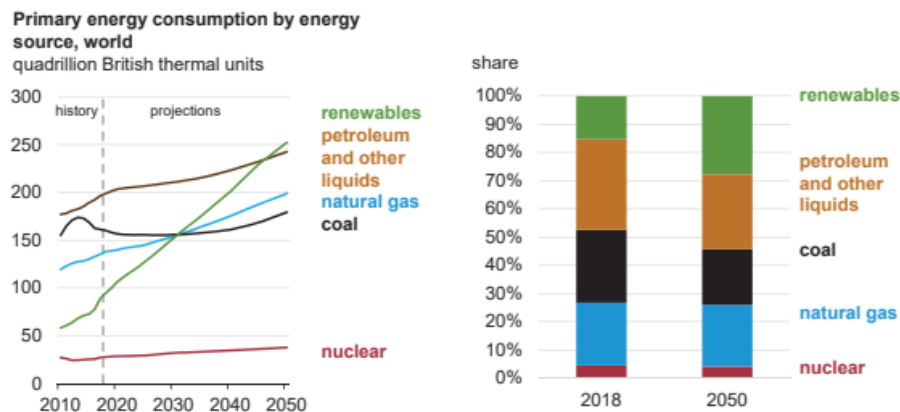
Figure 2: Left current consumption by various fuels with projections out to 2050. Right, the comparison of what percentage of each type of fuel makes up the total consumption in 2018 and for the 2050 projections [1]

The IEO also goes on to show that if look at only what is used in electrical production the amount of renewable energy would account for nearly 40% of the total world's electrical generation.

In the Reference case, most of the growth in electricity generation is fueled by renewables and natural gas—

Net electricity generation by fuel, world
trillion kilowatthours

Share of net electricity generation, world
percent
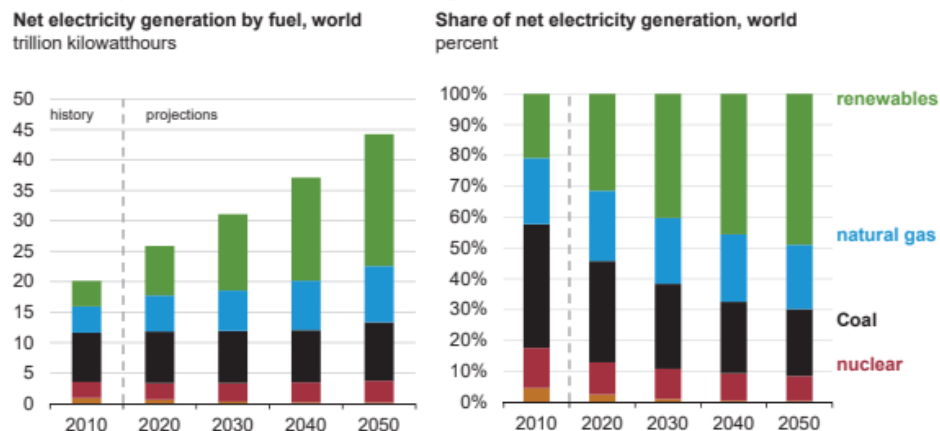
Figure 3: Left current and projected energy consumption if fuels solely used for electricity production. Right, the comparison of what percentage of each type of fuel makes up the total electrical production for current usage and projections [1]

This need for a reliable renewable energy sources is a growing interest of many industries. One such form of renewable energy that can be used both a macro and micro scale is solar energy. The IOE projection show, in figure 4 wind and solar energy will dominate the renewable energy field within the next thirty years.

Wind and solar dominate growth in renewables generation—

Net electricity generation from renewables, world
trillion kilowatthours

Share of net electricity generation from renewables, world
percent
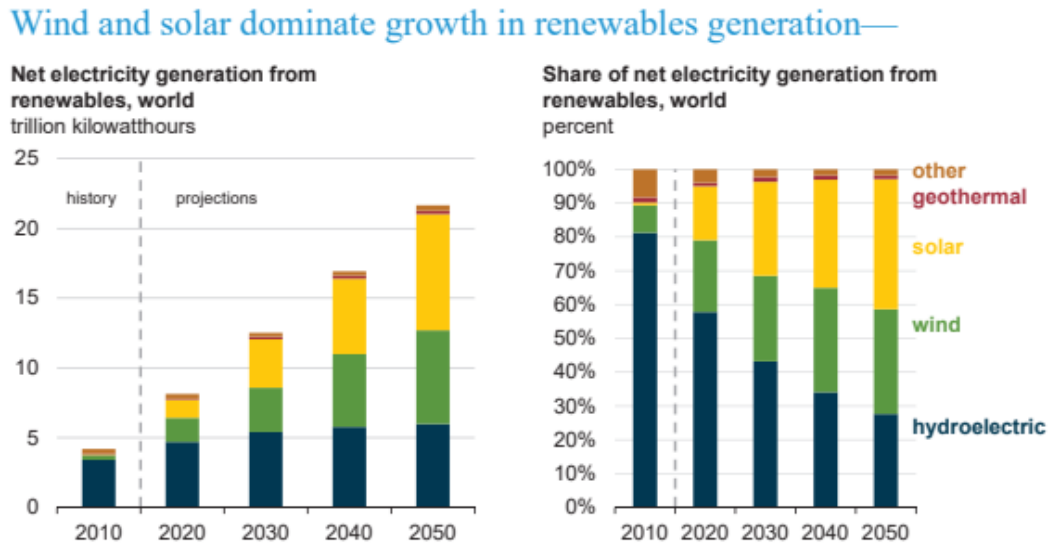
Figure 4: Left: break down of what forms of renewable electrical generation is consumed with projections to 2050. Right: the percentages of how much each renewable energy contributed to the total electrical production for current and projected data[1]

1.2   Forms Of Solar Energy Collection

Solar energy can be captured and used in many ways. Nearly everyone has made a solar cooker in their early education days. This simple device uses reflective surfaces to focus down light into a chamber where the food is held. . The concentration of light would heat the item within the chamber and cook it. In this use the solar energy is being converted into heat. This could be done on a large scale where the heat is captured in a fluid for use later. This is what is done at the Crescent Dunes Solar Energy Facility, which uses a concentrated solar power to heat molten salts [2].

Another form of solar energy is wind energy. This is an indirect form of solar energy as solar radiation heats the air causing it to rise. Since the total mass of the atmosphere, theoretically, remains constant cool air must move in to take the place of the rising hot air. The

kinetic energy of these wind currents are converted into electrical or mechanical energy by the use of wind turbines.

The issues with using wind turbines or concentrated solar power is that both of them are stationary and difficult to incorporate into an urban environment. These are the areas where solar cells can be used as a source of renewable energy. Solar cells are layers of light sensitive semiconductor materials. When these materials interact with light they generate electricity. Solar cells can be made in various sizes to accommodate the electrical need. Soar cells have a theoretical maximum efficiency of 33% [3]. Many commercially available solar cells come reasonable close to this theoretical efficiency. Solar cells can be used on massive solar farms or on the roof of a home allowing for both large scale and local energy production. One of the most common solar cells available is the monocrystalline silicon solar cells as seen in figure 5.

Figure 5: A wafer of monocrystalline silicon that is to be used in a solar cell [3]

Over time solar cells have developed from their rigid design to thin flexible design known as thin film solar cells. The design of the thin film solar cells makes uses of semiconductor layers that are only few micrometers thick. Thin film solar cells can be instilled on hybrid vehicles, backpack, or standalone personal unit.

1.3   Copper Indium Gallium Diselenide (CIGS) Solar Cell

A common type of thin film solar cell is the Copper indium gallium diselenide (CIGS) solar cell. These flexible cells use the CIGS compound as the primary active layer which generates the bulk of the current. The CIGS compound is a tetragonal chalcopyrite type crystalline structure shown in figure 6. [4]
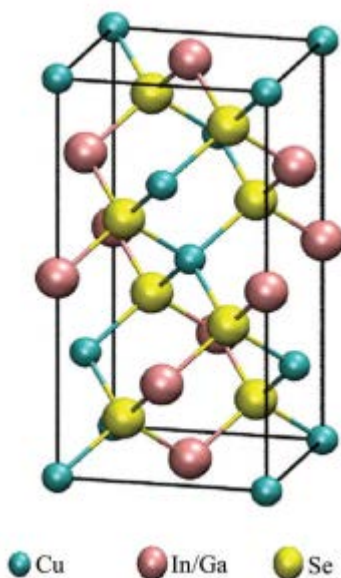
Figure 6: The unit cell of the CIGS molecule [4]

These solar cells are generally made out of five different layers. The top layer is made of zink oxide, ZnO and roughly 0.25 microns thick. Beneath that is a Cadmium sulfide. CdS layer, which is normally close to 0.07 microns thick. The middle layer, which is the primary active layer, is the CIGS layer which ranges between 1 and 2.5 microns. Beneath the CIGS is Molybdenum, Mo, layer which ranges between 0.5 and 1 micron thick. The Mo layer acts as a back contact and the ZnO acts as a transparent top contact region to which the electrons can flow somewhat laterally though to reach the metal contacts. Finally a back layer which is either

stainless steel or a glass sub straight is added. This bottom layer is primarily used for support of the others its thickness varies, displayed in figure 7[5].
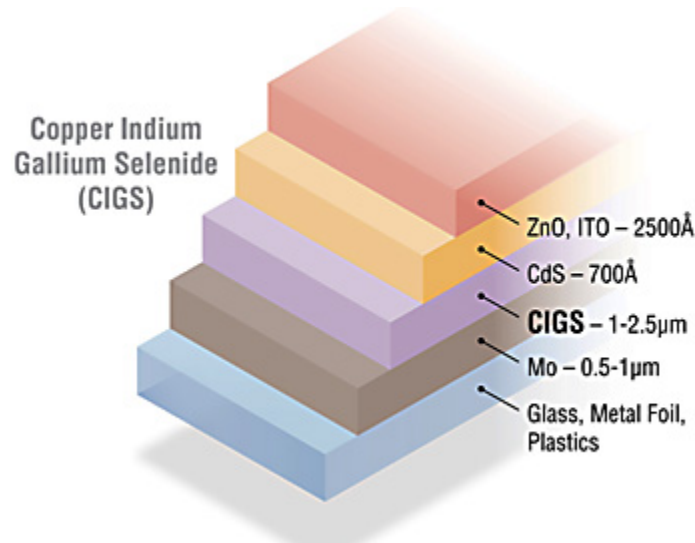
Figure 7: Diagram of the layers and thicknesses of a typical CIGS solar cell.[5]

Commercial solar cells are not always handled properly by the customers. Those that are installed on a roof top or a vehicle may not have regular maintenance or exposed to harsh weather conditions. The personal units would experience rough handling and improper set up on a bye use basis. These environmental and miss use factors solar cells must be made durable and withstand the stress caused by these factors. The stress caused by these factors can be simplified into three different loadings, tensile, bending, and rolling. By understanding how these stresses affect the solar cells performance would lead to better production and possibly more efficient and robust solar cells in the long run.

1.4   Literature Review

Understanding how stress affects the solar cell is important because it can alter the electrical properties of semiconductor materials. Semiconductor properties are dependent on their crystalline structure. Stress physically deforms the crystal structure of the active material resulting in an alignment mismatch. This mismatch has a direct effect on electron mobility and band gap separation [6]. Several reports have investigated how tensile, compressive, and bending

stresses affect a range of semiconductor-based devices. Moreover there are models that show how the electron mobility and material properties like it affect the solar cells performance.

Santhosh et al. [7] examined how mechanical tensile stress in silicon based solar cells may cause some degradation of the electrical properties but overall improve both the open circuit voltage and short circuit current of the cell. Salari et.al [8] showed that tensile applied strain in a roll-to-roll solar cell was found to increase the short circuit current by 3.8% when 2.4 mm of strain is applied, beyond this strain there is a reduction in short circuit current. This short circuit reaction was found to be inversely related to the series resistance and slight relation to the shunt resistance. Ungersboeck et al. [9] showed that arbitrarily applied stress in silicon based electrical devices can undergo electron mobility enhancements, thus improving the performance of the component. Kang [10] had shown that both tensile and compressive uniaxial strain on Silicon based MOSFETs caused a narrowing of the band gap as well as a non-negligible change in the carrier mobility, both of which will affect the performance of the MOSFET.

Lee et al. [11] also executed bending tests of Pbs/Cds thin-film solar cells by applying a load between two parallel holders. They reported that the short circuit current decreases drastically above a certain bending strain, while open-circuit voltage is not much influenced by the bending strain. They also found that the density of the surface layer cracks was depending on the deposition temperature that took place during the fabrication process. The deposition temperature dependence was explored by Kim et al. [12]. He performed finite element simulation of thermo-mechanical stress of CIGS solar cell produced by cooling down to room temperature from various annealing temperatures (200 °C – 400 °C). Their CIGS solar cell is composed of ZnO, CdS, and CIGS active layers. They found that CIGS solar cells have compressive residual stress in ZnO and CdS layers when the cell is cooled down to room temperature after high temperature annealing. They also found that upper part of CIGS layer of the cell is in tensile stress while the lower part of CIGS layer is in compressive stress. Kim et al [13], had also found that cracks along the grain boundaries of the CIGS solar cells decreases the overall performance by reduction of the open circuit voltage through the uses of a 3D finite element simulation. His results though not the same as those found by Lee, shows that crack degradation plays an important role in the performance of thin film solar cells. Wiedeman [14] extended the bending tests by rolling CIGS solar cells around a mandrel. Cells were examined in

both compressive (grid toward mandrel) and tensile (grid away from mandrel) stress, he reported that compressive stress causes more damage than tensile stress, and that a bend radius less than 0.25 inch shows a rapid increase in damage to the cell's performance.

I few of the previous papers have discussed how stress or strain can affect the electron mobility or the electron life time. Haque et al.[15] has shown through an analytical approach that the reduction in the product of electron mobility and electron life time reduces the short circuit current density, while a reduction in the product of whole mobility and hole life time reduces the open circuit voltage. Rahim et al [16] has also found similar results. They reported that reduction in electron life time reduces the short circuit current and reduction in hole life time reduces the open circuit voltage. That also found that the hole life time has grater impacts on the performance than the electron life time. Nobel et al [17] had shown that with increasing dislocation, brought about by the addition of geranium into hydrogenated amorphous silicon solar cells, a reduction in electron mobility and the shifting of the Fermi-level closer to the conduction band takes place. This shows that physical changes such as an increase in dislocations, can affect properties such as electron mobility.

There are not many papers that are able to tie the effects of stress to both a solar cell performance and its intrinsic material properties. This is what is approached within this report. Chapter two will go into the history and derivation of the theoretical components of semiconductor devices as well the meaning behind measureable parameters, and a brief segment about stress and strains. Chapter three will cover the experimental procedures for collecting solar cell performance, the axial tensile stress, Bending stress, Rolling stress, and derivation of light intensity distribution equation that was used to perform the experiments. Chapter four covers the reasoning and procedures for the simulated modeling that was done in Matlab and COMSOL Multiphysics. Chapter five covers the results of the three different applied stress experiments as well as the simulated results. Finally Chapter six raps up all the results and discuss possible areas the research may continue into.

2. THEORY

2.1 Brief History Of Semiconductor Derivation

2.1.1 Photoelectric effect

All solar cells operate off the basic theory of the photoelectric effect that was first described by Albert Einstein in 1921, which he would receive the Nobel prize for the following year [18] . In it he explains how electrons can be excited across a gap between two metal plates by the use of a light source. Most notable about these experimental results is that he had found the intensity of the light source did not create an increase of escaped electrons, but the frequency of light did [19]. Since the frequency of light is directly related to the energy of light through the plank's constant.

$$E = hf$$

The implication of the energy restriction range is that only select energies can be accepted by the electrons and grant them freedom from the plates. This restriction of energies as dubbed a quanta of energy, a discretized packet of acceptable energies which is taken in by the trapped electrons. This paper also went on to explain the work function of expectable energies. The work function being the amount of energy needed to break the electrons out of main body of the material to where it can be considered a free electron. The area outside of the material is known as a vacuum [20].

2.1.2 Quantum mechanics expansion

This concept quanta was later expanded on with the application of quantum mechanics to the simplified single particle in a box problem. Through that mathematically approach it was found that only certain energy states can be aloud, as such only certain imputes of energies can be accepted to reach the next energy state. This model was successfully applied to the hydrogen atom and predicted its color spectrum. This model was also used to describe what quanta of energy is needed to completely remove an electron from its well, in the case of the hydrogen atom this amount of energy was the same as its work function [21]. This model was further applied to a few other atoms on the periodic table and many other applications. Currently a modified version of this

the single particle in a box is being used to model the quantum well of an atoms nucleus in hopes of finding the next stable heavy element [20].

2.1.3   Thermo physics expansion

The single particle in a box theory has its draw backs in only being able to incorporate a small handful of particles at once. To expand this to a large collection of particles, enough to be considered a physical object the application of thermo physics was needed. Through the uses of a k-space, that is a three-dimensional space with energy and states for axis, it was found that an energy sphere is formed when all particles of a given type, within a chunk of mater, are in the lowest possible energy state [22]. Since no more than two particles like an electron can exist in a single energy state you end up getting a stacking effect of the energy states. The outer most filled energy state, of these compacted levels, is known as the Fermi-level. This Fermi-level only completely filled at absolute zero, at higher temperatures a number of electrons free to move within the bulk material so long as they are not bound within the crystal lattice. This distribution of free electrons and bound electrons creates two sets of energy bands [23]. A filled set of energy states below the Fermi-level, comprised of bound electrons, that makes the valence band. The other set of a collection of free electrons within the bulk of the material, these collections of energy states is usually above the Fermi-level and is known as the conduction band. Ideally the Fermi-level sits with in the middle of a band gap. The band gap, E_G, is a region between the highest energy state in valence band E_V, and the lowest energy state in the conduction band, E_c . Normally this band gap is a region where electrons cannot occupy. This region is commonly known as the band gap and is found by the deference of the two band edges.

$$E_G = E_c - E_V$$

The valence band is typically depicted as a set of bands lines stacked on top of each other to create a band of a given thickness. This method was also used to find the energy levels that would result in an electron being broken from the material bonds and existing freely within the bulk of the material. This analysis forms the conduction band.
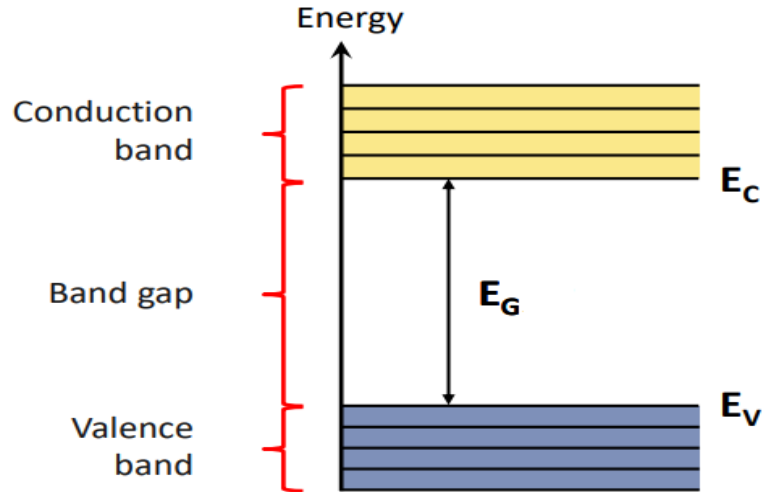
Figure 8: A diagram of the conduction, valence, and band gap for a semiconductor material.[3]

The energy levels for the conduction band edge and valence band edge are defined by using the electrostatic potential, $\emptyset$, and the electron affinity χ.

$$E_c = -(\emptyset + \chi)$$
$$E_V = -(\emptyset + \chi + E_G)$$

The electron affinity is defined at the amount of energy needed to remove an electron from the conduction band edge and bring it out of the bulk material where is will be a free electron in a vacuum.
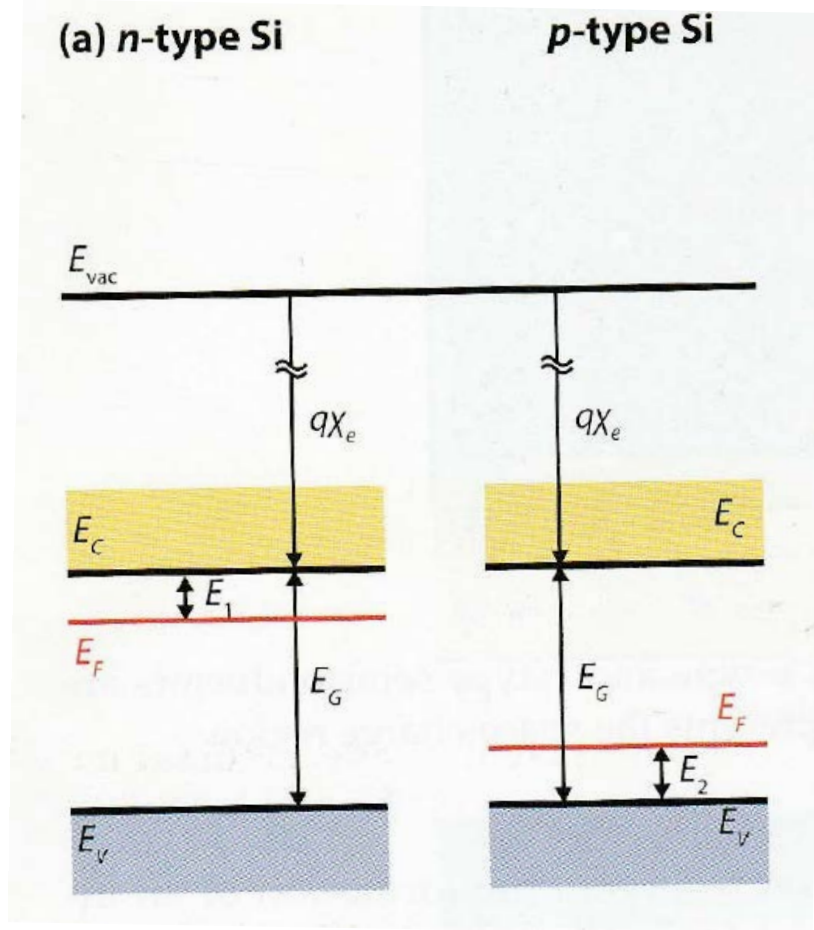
Figure 9: Diagram of conduction and valence band for a n-doped (left) and a p-doped (right) semiconductors. Both show the Fermi-levels and the electron affinity[3]

The band gap, electro static potential, and the electron affinity can all be measured experimentally. With these know the valence band and the conduction band edges can be found.

2.2 Solid State Physics Expansion

Solid state physics took things a step further. It tied the existing concepts with the properties and physical concepts of matter. Through this it was able to tie various electrical, thermal, and mechanical properties to the crystalline properties of various materials. For solar cells the material under consideration are photosensitive semiconductors.

2.2.1   Governing semiconductor equations

Using the concepts of the valence, gap, and conduction bands as well the Maxwell equations for electrodynamics, one can explain the motion of electrons and holes through a material and its different energy bands. Through this application the Poisson equation and the Electron-hole continuity equations could be derived. These questions are the governing electrodynamics equations for semiconductor devices. The Poisson equation relates the electrical potential to the charge density and is given by:

$$\nabla \cdot (\varepsilon \varepsilon_0 \nabla \emptyset) = -\rho$$

Where, $\emptyset$: Electrostatic potential, ε_0 is the permeability of free space, ε is the material permeability, and ρ is the charge density. This equation states that the second spatial gradient of the electrostatic potential is proportional to the negative of the charge density [24]. The charge density is the summation given by:

$$\rho = q(n - p + N_A - N_D)$$

Here, N_A: acceptor concentration and N_D: donor concentration, n: is the electron density, p: is the hole density, and q: is the fundamental electric charge. This equation simply states that the charge distribution has contributions from the electron density and accepter concentration of the material, and a reduction of charge density from the hole density and the donor concentration.

The electron-hole continuity equations relate the change in a type of charge to the sources of charge in that region and if given by:

$$\frac{\partial n}{\partial t} = \frac{1}{q} \nabla \cdot J_n - U_n + G_n$$

$$\frac{\partial p}{\partial t} = \frac{1}{q} \nabla \cdot J_p - U_p + G_p$$

Where, U_n: recombination rate for electron, U_p: recombination rate for hole, G_n: generation rate for electron, G_p: generation rate for hole, J_n: electron current density, J_p: hole current density, n: electron concentration, p: hole concentration. These to equation state the time dependent change in the electron and hole densities are governed by the gradient of their respected current densities, with contributions from their respective generation rates, and reductions from their respective recombination rates [3].

2.2.2 Transport equations

The electron and hole current densities used in the continuity equations are derived from the addition of the drift and diffusion current densities. These currents describe real partials traveling through the crystalline lattice structure of the semiconductor; as such they are susceptible to temperature [25]. This is because at higher temperatures there are more vibrations of the lattice structure, which are given by:

$$J_n = qn\mu_n\nabla E_c + \mu_n k_b T\nabla n + qnD_n\nabla \ln (T)$$
$$J_p = -q\mu_p n\nabla E_V + \mu_p k_b T\nabla p + qpD_p\nabla \ln(T)$$

Where, T: is the fundamental temperature, μ_n: electron mobility, μ_p: hole mobility, D_n: Diffusion coefficient of electron, D_p: Diffusion coefficient of hole and diffusion coefficient are defined by the equation, $D/\mu = k_B T/q$, where $k_B T/q$ is the thermal voltage. This version of the of the electron and hole current density equations do not take into account the effects of magnetic fields though.

2.2.3 Mobility, life time, and Shockley-Read-Hal

The electron and hole mobility appear more than once within both current densities and have a direct relation to the diffusion coefficients. The mobility is a key part in the current densities since it is a descriptor of how well an electron or hole can move through the semiconductor material [26]. It's found by dividing the thermal velocity, or drift velocity, v, by the electric field.

$$\mu = v/\emptyset$$

Another important parameter is the electron life time, and hole life time. Given by:

$$\tau_{n,p} = (v_{th}\sigma_{n,p}N_{defect})^{-1}$$

Where, σ: is the capture cross sections, which describe how far an electron or hole can travel before encountering a defect, N_{defect} is the density of acceptor or donor defects within the lattice, and v_{th} is the thermal velocity.

2.2.4 Shockley-Read-Hall trap-assisted recombination/generation

The life time plays a key role in the in generation potion of the Shockley-Read-Hall(SRH) or trap-assisted recombination/generation. Solar cells are made from layering the semiconductor materials to create a photo-sensitive diode. These diodes do not behave ideally and as a result a

certain amount and method of recombination/generation takes place within them due to these defects. The SHR recombination/generation method makes uses of an intermediate accessible energy state within the band gap. This intermediate state acts as a trap for electrons and holes as it cycles though a four stage process of recombination and generation [3].

1.   An electron loses energy as thermal vibrations and drops from the conduction band to the trap

2.   From the trap the electron loses energy once more dropping down to the valence band and recombining with a hole.

3.   An electron hole pair is made with the electron being excited into the trap.

4.   Additional energy is added to further excite the electron into the conduction band.

The net carrier, electrons and holes, generation/recombination is given by:

$$G_{net} = \frac{(np - n_i^2)}{\tau_p(n + n_1) + \tau_n(p + p_1)}$$

n_1, and p_1 are given by,

$$n_1 = n_i e^{\left(\frac{E_t - E_i}{k_B T}\right)},$$

$$p_1 = n_i e^{\left(\frac{E_i - E_t}{k_B T}\right)},$$

And

$$n_i = \sqrt{N_c N_v} e^{\left(\frac{-E_g}{2 k_B T}\right)},$$

Where, E_t=trap energy level, n_i= intrinsic carrier concentration, N_t=trap concentration, N_c=effective density of state of conduction band, N_v=effective density of state valance band. Generation and recombination are determined by the sign of G_{net}. Sign is positive for generation and negative sign for recombination.

2.2.5   Measurable properties of a solar cell.

Since solar cells behave in a manner similar to diodes, the values of the short circuit current, I_{sc}, as well as the open circuit voltage, V_{oc}, can be used to measure its performance. If we look at the short circuit current, it's the current when the voltage is non-existent, using the general form

for the total current in the cell, it is found that ideally the short circuit current should match the photo generated current.

$$J = -J_{rec}(V) + J_{gen}(V) + J_{ph}$$

Or

$$J = J_0 \left(e^{\left(-\frac{qV}{k_bT}\right)} - 1 \right) + J_{ph}$$

Where, $J_{rec}(V)$: is the recombination current density as a function of voltage, $J_{gen}(V)$: is the generation current density as a function of voltage, J_{ph} is the photo-generated current, V is the applied voltage, J_0 is the dark circuit current. The photo-generated current and the dark current are derived from the physical properties of the diode materials. They are given by:

$$J_{ph} = qG(L_N + W + L_P)$$

$$J_0 = qn_i^2 \left(\frac{D_n}{L_N N_A} + \frac{D_p}{L_P N_D}\right)$$

Where, G: is the generation rate, $D_{n,p}$: are the diffusion coefficients for electrons and holes respectively, $L_{N,P}$: are the diffusion lengths for the electrons and holes, $N_{A,D}$: are the number of acceptors and donors within the material, and W is the width of the depletion region. The depletion region is a physical area where no holes or electrons freely exist. This is because of the built in voltage that accrues when the p-doped and n-doped semiconductor that make up the diode come in contact. Looking at wither of these equations on can see that when the voltage is zero the short circuit current would ideally be the same as the photo generated current.

The second measurable parameter is the open circuit. This is the voltage given when no current can run through it. It is given by:

$$V_{oc} = \frac{k_bT}{q} \ln\left(\frac{J_{ph}}{J_0} + 1\right)$$

The photo generated current tends to stay constant though, as a result the V_{oc} can be considered a function of the dark current density.

The maximum power can be measured as well and is given by:

$$P_{max} = V_{max} \times I_{max}$$

There are two kinds of efficiency that can be measured. The first is the external quantum efficiency, this method examines output photo generated current over the input photon flux at a given wavelength multiplied by the fundamental charge [3]. This provides the efficiency of the

solar cell at a given wavelength of light. By measuring this value over several different wavelengths one can find the effect of wavelength on this form of efficiency and, with the proper set up, can identify sources of parasitic absorptions, and optical effects of the solar cell. This method does require a reference value to determine the initial flux of light, for this a calibrated light sensitive diode is used. With the consideration of this reference value the external quantum efficiency is given by:

$$EQE(\lambda) = EQE^{Ref}(\lambda) \frac{I_L(\lambda)}{I_L^{Ref}(\lambda)}$$

The first method of efficiency is difficult to obtain during stress induced experiments, so the efficiency was measured by the second method. The second method using the maximum power as well as the standard input power of P_o=1000 W/m^2, and the surface area the efficiency of the cell can be obtained by:

$$Eff = \frac{P_{max}}{P_o A} = \frac{V_{max} \times I_{max}}{P_o A}$$

Where, A is the area of incidence.

Then there is the fill factor, which is a measure of the cells usable potential. The current and the voltage are the largest as the short circuit and open circuit conditions respectively. In theory the largest power, the cells full potential, would come from the product of the two. Since this is not possible, the maximum power is divided by the product of the short circuit current and the open circuit voltage.

$$FF = \frac{V_{max} \times I_{max}}{V_{oc} \times I_{sc}}$$

2.2.6 Physical meaning of measured parameters

The typical current voltage (I-V) curve of a solar cell is found by applying various voltages and measuring the output current [27]. As seen is figure 10, the short circuit current is found at the intersection of the plot with the current axis. The Open circuit voltage can be seen in the same figure being found where the plot intersects the voltage axis.
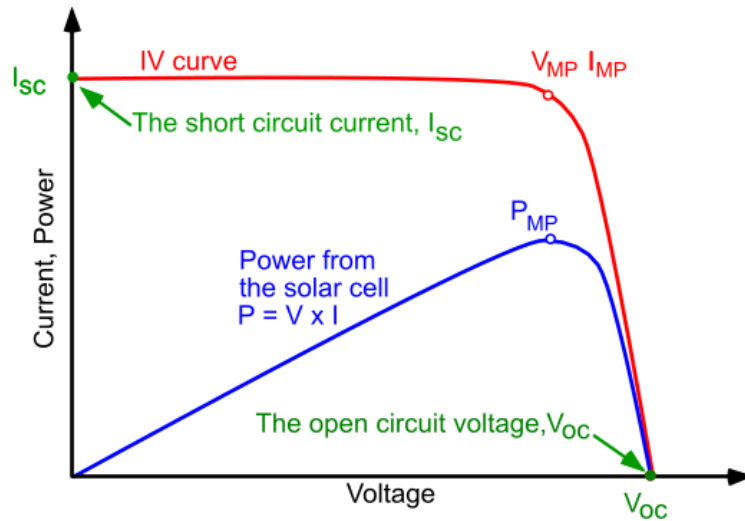
Figure 10: A typical current-voltage curve that Is obtained during solar cell testing. Superimposed on this graph is the power-voltage curve [27]

Figure 11 gives the physical representation of maximum power and the fill factor. The fill factor can be described graphically as a measure of how square the plot is [27]. The closer this value is to one means the cell is capable of being closer to its theoretical maximum.
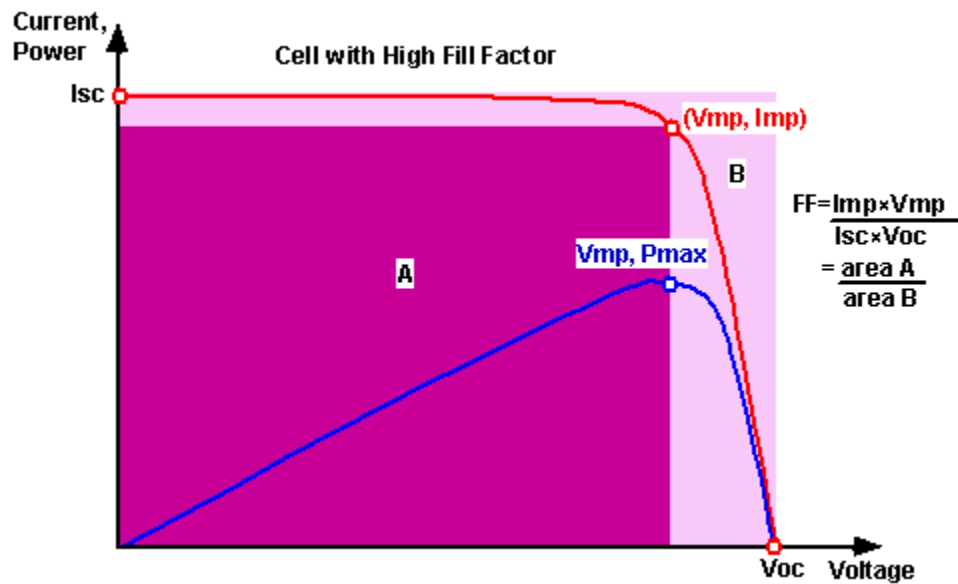
Figure 11: The visual depiction of how the fill factor measures the "square-ness" of the I-V curve [27]

2.3   Physical Importance Of Stress On Crystal Structures

2.3.1   Generalities of stress

All these parameters are dependent on the crystalline and electrical properties of the material. If the crystalline structured is altered or damaged it would lead to a change in parameters and thus effecting the performance of the solar cell [6]. Changes to the materials structure can arise through applications of stress. This paper focuses on applications of mechanical stress. Stress, β, is defined as the applied force, F, divided by the cross sectional area.

$$\beta = \frac{F}{A}$$

The application of stress results in a deformation of the material. The measurement of this deformation is strain. If the force is applied along single axes and places the material in tensile loading, the material will elongate in that direction while contract along the other two axes [28]. The Strain, γ measures the amount of deformation by dividing the change in length, ∇l, by it's original length, l_o.

$$\gamma = \frac{\nabla l}{l_o}$$

When this is applied to the Nano-level, the level of atoms, atomic bonds, and crystal structures, it has a more profound effect. On this scale the deformation is the shifting of atoms within the crystal. Grains may slide past each other or reorient themselves. Looking at the actually crystal lattices a sheet of or string of atoms may break from the lattice bonds and slide over the others and make new bonds in this new alignment Figure 12 shows this for applied shear stress and a slip plane within the crystalline structure[28].
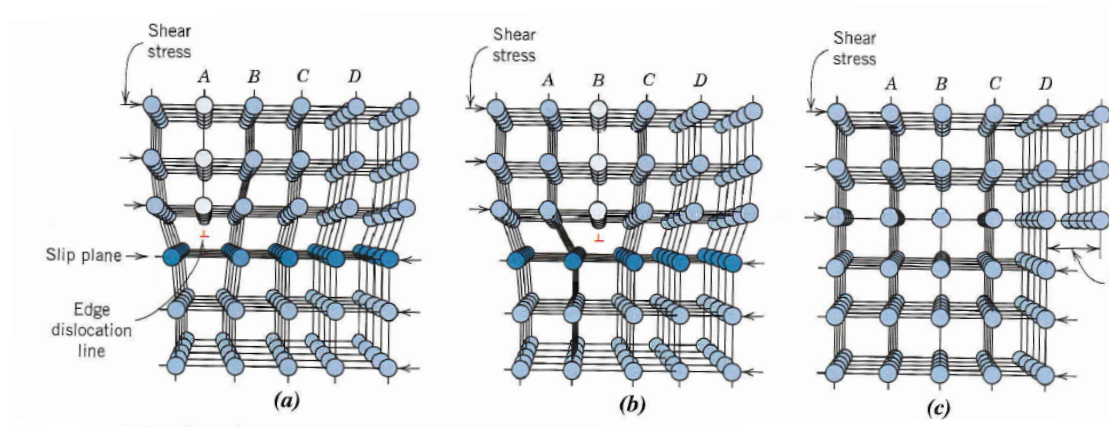
Figure 12: A visual depiction of how a load may cause a slip plane in the crystalline structure to move and alter the crystalline structure.[28]

2.3.2   Stress in solar cells

As mentioned in the previous section the stress causes physical changes in the crystalline structure of a material, and many parameters for a solar cell are dependent on the materials physical make up and structure: these include the electron and whole mobility which plays a role in the current density, a the electron and hole life times which play a role in the SRH recombination an generation of charge carriers. As the crystal reforms these vales would change and is believed to result in degradation of the cells.

3. EXPERIMENTAL PROCEDURE

3.1   Basic Data Collection Of I-V Curve

For all experiments the Hanergy SP-08 flexible CIGS solar was used. The first step was the preparation of the solar cell. First the leads had to be exposed. This was done by removing the USB port and its housing. Once this was complete the cell was placed in in the MTS universal testing machine to maintain an upright position. A thermocouple was taped to the back center of the solar cell and the leads were connected to a solar analyzer.

To maintain standard testing of 24 ^{o}C a fan was place beside it and set to its second speed. The purpose of the fan is to prevent over-heating of the solar cell, on this setting the fan is able to hold temperature of the cell around 24°C ± 1°C. To meet the 1.5AM solar radiation standard the cell is constantly illuminated by a tungsten halogen lamp. A standard of 1000 W/m^2 intensity over the cells surface was required as well. This was achieved by precise placement of the lamp so it generated an average 1000 W/m^2 over the cell. This location was selected be a set of equations that described the intensity distribution over the cells surface, which will be discussed in the next section.

The cell was left in this state of illumination for thirty minutes to allow for temperature, and electrical fluctuations to stabilize before any experiment began. The electrical performance of the cell was measure using a solar analyzer: Open circuit voltage (V_{oc}), Short circuit current (I_{sc}), Efficiency (EFF), Fill factor (FF) and Current-Voltage curve (IV curve).
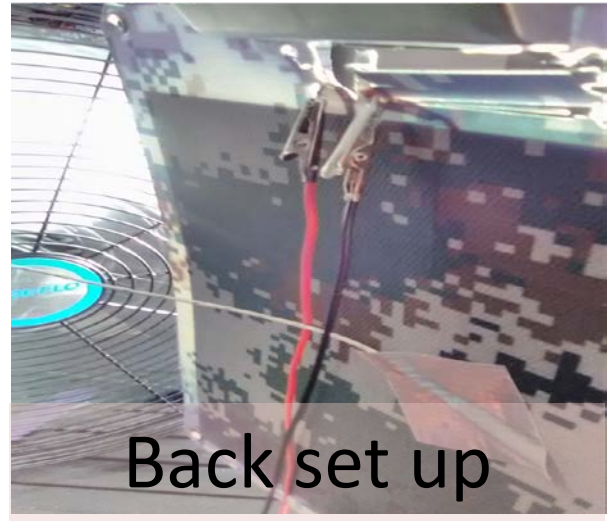
Figure 13: Left set up of all equipment for general collection of solar cell performance. Right the set up for how the leads and thermistor are attached to the cell.

3.2   Location Of Light Source Equations

The intensity of light is given by.

$$S = \frac{S_o}{4\pi d^2}$$

Where S_o, is the intensity of the point source and d, is the distance from the source. Normally the light source is at such a great distance from the solar cell that it is assumed to be uniform over the entire area of the cell. However this is not the case with using a lamp fixture in close proximity to the cell. The distance from the closest point on the cell will be notably different from the point furthest from the cell. Because of this variation an equation is needed that can describe these intensity gradients across the cell.

This starts with using the distance equation for d. For this we will assume that the light source is placed some distance along the negative y-axis, with the center of the cell located somewhere along the positive y-axis, as shone in the figure 14.
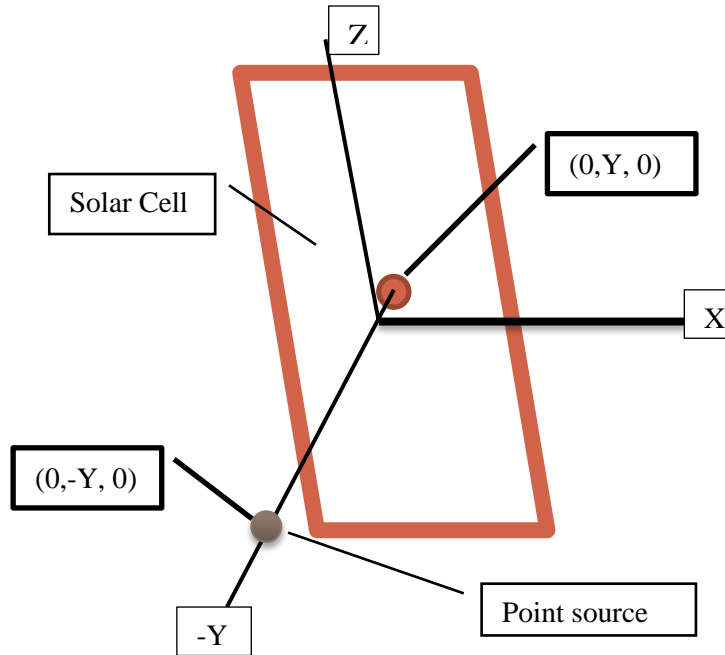
Figure 14: Diagram of how solar cell and light source is placed in a three-dimensional coordinate system

To start we will rewrite d in terms of the distance equation.

$$d = \sqrt{x^2 + y^2 + z^2}$$

To simplify this we look try to reduce this down to a two variable equation at most. Start with looking at the above view of the solar cell in the xy plane in figure 15.

a   B
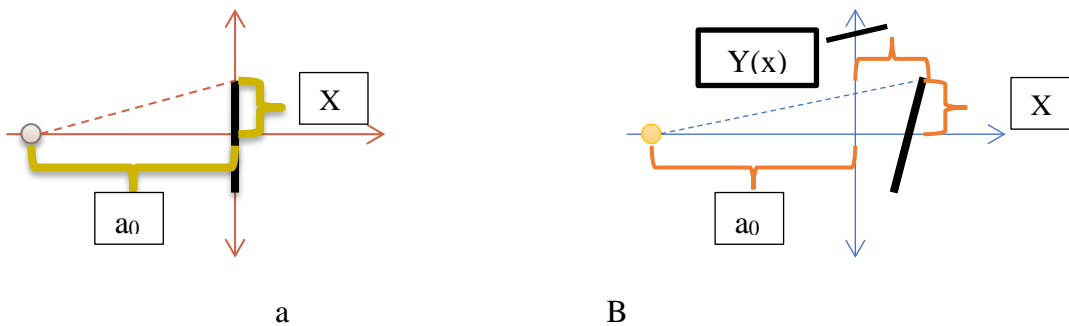
Figure 15: a) Cell aligned with x-axis and centered on the y-axis. b) Cell only centered on the y-axis

From the diagram it is seen that with a light source fixed at a given location has a constant distance from the x axis given as a_0. This constant distance still remains even if the cell is not

aligned with the x-axis. The distance from the x-axis to the cell can be written as a function of x, as the location of the cell. In the case figure 15 the equation would be for that of a straight line and have the form of y=mx+b. Though that may not be the case, the cell might be curved, in those instances a parabolic, quadratic, a segmented polynomial, or even an exponential curve can be used. So long as it accurately describes the location of the cell in the xy-plane. This means the total distance along the y-axis can be written as a constant plus some function of x.

This gives

$$d = \sqrt{x^2 + (a_o + y(x))^2 + z^2}$$

And

$$S = \frac{S_o}{4\pi\sqrt{x^2 + (a_o + y(x))^2 + z^2}^2} = \frac{S_o}{4\pi(x^2 + (a_o + y(x))^2 + z^2)}$$

Another issue that arises with a close proximity light source is the angle of incidence. Normally a light source that has traveled a great distance has very little deviation due to angle and can, in theory, have the entire exposed area of the cell exposed to a light of uniform incidence at the angle that produces the most output. For a close proximity light source there is a gradient of incidence angles that must be accounted for. This angle reduces the intensity that can be accepted by the cell.
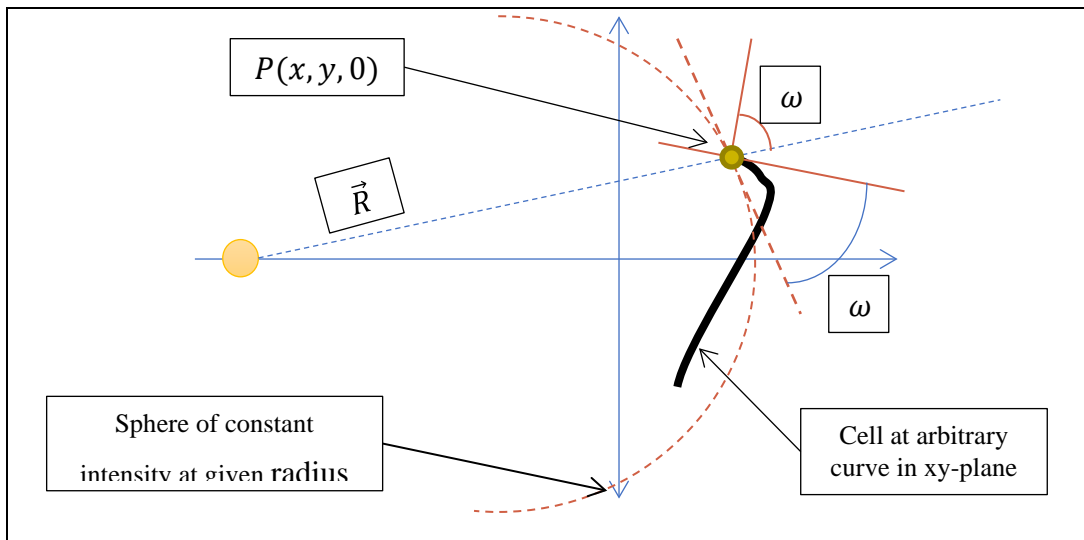
Figure 16: Diagram for finding the angle of incidence for a ray of light and the surface of the solar cell with an arbitrary curve in the xy-plane at a given point P(x,y,0)

To find out the amount of absorbed light, assuming the cell absorption if hundred percent when the light ray is normal to the cell's surface, one would need to know what portion of the incident light ray was normal to the cell. To do this the incident light ray will be projected onto the normal to the cell surface at a given point. The projected intensity is given by:

$$S_{n(xy)} = S \cos \omega$$

The made between the normal of the cells surface and the ray of light is the same angle as the angle between the tangent line of the cell's curve at that point, and the tangent line to sphere of constant intensity, made at the given radius of R, and lies in the xy-plane. This angle can be found with the equation:

$$\omega = \tan^{-1}\left(\frac{m_2 - m_1}{1 + m_2 m_1}\right)$$

The slopes for m_1 are the slop of the tangent to the sphere of constant intensity in the xy-plane. This slope is the inverse slope which the light ray makes with respect to the xy-axis, because it is normal to the sphere and the spheres tangent. This gives m_1 to be:

$$m_1 = -\left(\frac{y_2 - y_1}{x_2 - x_1}\right)^{-1}$$

For the arbitrary curve of the cell the slope must be found through the derivative of the equation describing the curve at that point.

$$m_2 = \frac{dy}{dx}\Big|_{p(x,y,0)}$$

This leads ω, to be

$$\omega = \tan^{-1}\left(\frac{\frac{dy}{dx}\Big|_{p(x,y,0)} - \left(-\left(\frac{y_2 - y_1}{x_2 - x_1}\right)^{-1}\right)}{1 + \frac{dy}{dx}\Big|_{p(x,y,0)}\left(-\left(\frac{y_2 - y_1}{x_2 - x_1}\right)^{-1}\right)}\right)$$

The intensity absorbed from the point source also depends on the angle of incidence in the z direction ω_2 as well. If one assuming that the eight of the cell, h, is a function of z then following a similar processes the ω_2 will be given by:

$$\omega_2 = \tan^{-1}\left(\frac{\frac{dh}{dz}\Big|_{p(x,y,z)} - \left(-\left(\frac{z_2 - z_1}{P(x,y,z)_2 - P(x,y,z)_1}\right)^{-1}\right)}{1 + \frac{dh}{dz}\Big|_{p(x,y,z)}\left(-\left(\frac{z_2 - z_1}{P(x,y,z)_2 - P(x,y,z)_1}\right)^{-1}\right)}\right)$$

This gives the simplified form of the useable light intensity by:

$$S_{n(xyz)} = S \cos \omega \cos \omega_2$$

Substituting in the equations for S, ω, and ω_2, as well as applying the conditions that the center of the cell is aligned with the coordinate center as well as the x and z axis, the usable light intensity becomes.

$$S_{n(xyz)} = \frac{S_o \cos\left(\tan^{-1}\left(\frac{x}{a_o}\right)\right) \cos\left(\tan^{-1}\left(\frac{z}{\sqrt{x^2 + (a_o)^2}}\right)\right)}{4\pi \left(x^2 + \left(a_o + \sqrt{(a_0)^2 + x^2}\right)^2 + z^2\right)}$$
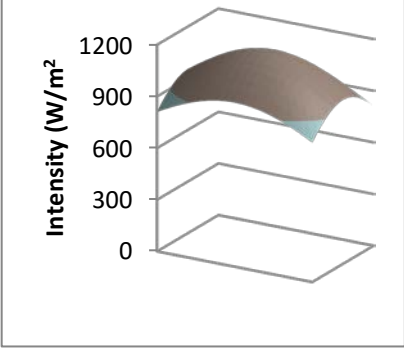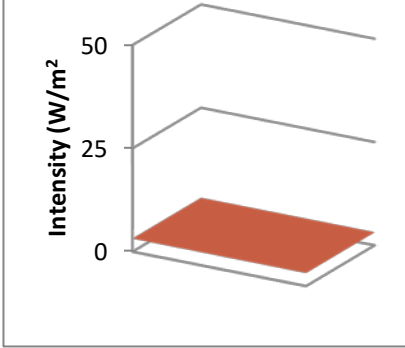
Where, S_o was determined by measuring the intensity of the light with light meter at a fixed distance from the tungsten halogen lamp. Using these measurements S_0 was found by.

$$S_o = 4\pi S d^2$$

This gave the intensity of the point source a value of 1180 Watts.

These equations for usable light intensity was programed into excel and the intensity was found at 247 evenly spaced points across the surface of the solar cell. The average and standard deviation of this data set was found. The goal seek function in excel was used in find the value of a_o, the distance the lamp is from the cell, for two cases. The first case is when the standard deviation is zero; this means all points of the cell experience the same intensity. The second case used the goal seek to find the value of a_o that would produce an average value of 1000W/m^2 over the surface of the sell.

Table 1: Output from usable intensity equation

parameter	Intensity 1000 W/m² restriction	Standerd deviation 0 W/m² restrictions
Graphical representation of intensity across the cell surface		
Intensity W/m²	1000	3.178624
Standard deviation W/m²	82.47882	0.000818
Lamp distance m	0.286509214	5.434104304

The outputs from the usable light intensity equation show that in order to get a uniform distribution of light across the cell, the light source has to be placed 5. 43m to be uniform, but will have an average intensity 3.18 W/m². Without a stronger lap to serve as the point source the 5.43m distance was not used. The average intensity of 1000 W/m² was used with a lamp distance of 0.287m, approximately 11.4 inches, from the surface of the cell for all experiments.

In the case of a curved solar cell that forms an arc with radius of r_c and in one of two specific positions based on a convex of concave curvature can be described by using the equation of a circle that is off set along the y-axis by

$$y(x) = \begin{cases} +\sqrt{(r_c)^2 - x^2} + K, & concave, K = D - r_c \\ -\sqrt{(r_c)^2 - x^2} + K, & convex, K = -r_d \end{cases}$$

Where K is the y-axis off set and is the depth of the arc made by the curved cell. The radius of the cells was found by measuring the width, W, and depth, D, of the arch made by the cell and using the intersecting chord theorem gives.

$$r_c = \frac{4D^2 + W^2}{8D}$$

The specific positions of the concave and convex cells that are governed by these equations can be seen in the figure 17 below.
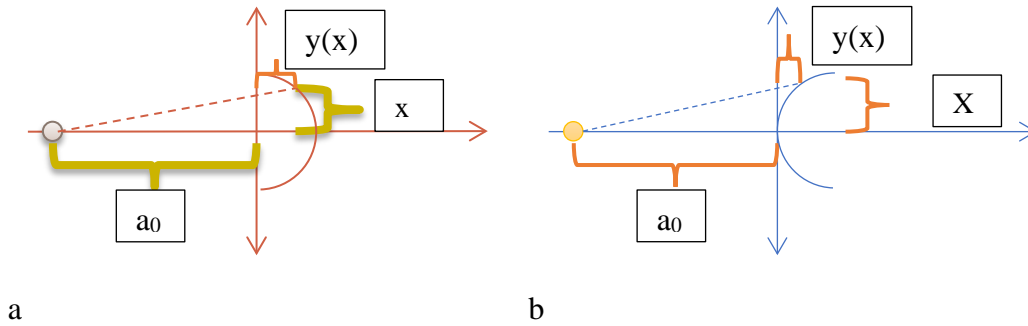
Figure 17: a) Concave cell aligned with x-axis and centered on the y-axis. b) Convex cell aligned with x-axis and centered on the y-axis

These configurations change the distance the light source needs to travel as well as the slopes that are used. The new light source distance is given by.

$$d(x,z) = \begin{cases} \sqrt{x^2 + \left(a_o + \sqrt{(r_c)^2 - x^2} + K\right)^2 + z^2}, & concave \\[2em] \sqrt{x^2 + \left(a_o - \sqrt{(r_c)^2 - x^2} + K\right)^2 + z^2}, & convex \end{cases}$$

The inverse slope of the light ray in a given xy-plane is given by

$$m_1 = \begin{cases} \dfrac{-x}{\sqrt{(r_c)^2 - x^2} + K + a_o}, & concave \\[2em] \dfrac{x}{\sqrt{(r_c)^2 - x^2} + K + a_o}, & convex \end{cases}$$

The inverse slope at a point on the cell in the xy-plane is given by

$$m_2 = \begin{cases} \dfrac{-x}{\sqrt{(r_c)^2 - x^2}}, & concave \\[2em] \dfrac{x}{\sqrt{(r_c)^2 - x^2}}, & convex \end{cases}$$

43

Plugging the new light source distance and the new slopes into the intensity equations gives.

$$f(x) = \begin{cases} \dfrac{S_o \cos\left(\tan^{-1}\left(\dfrac{\left(\dfrac{-x}{\sqrt{(r_c)^2 - x^2} + K + a_o}\right) - \left(\dfrac{-x}{\sqrt{(r_c)^2 - x^2}}\right)}{1 + \left(\dfrac{-x}{\sqrt{(r_c)^2 - x^2}}\right)\left(\dfrac{-x}{\sqrt{(r_c)^2 - x^2} + K + a_o}\right)}\right)\right) \cos\left(\tan^{-1}\left(\dfrac{z}{\sqrt{x^2 + (a_o)^2}}\right)\right)}{4\pi\left(x^2 + \left(a_o + \sqrt{(r_c)^2 - x^2} + K\right)^2 + z^2\right)}, & concave \\[4ex] \dfrac{S_o \cos\left(\tan^{-1}\left(\dfrac{\left(\dfrac{x}{\sqrt{(r_c)^2 - x^2} + K + a_o}\right) - \left(\dfrac{x}{\sqrt{(r_c)^2 - x^2}}\right)}{1 + \left(\dfrac{x}{\sqrt{(r_c)^2 - x^2}}\right)\left(\dfrac{x}{\sqrt{(r_c)^2 - x^2} + K + a_o}\right)}\right)\right) \cos\left(\tan^{-1}\left(\dfrac{z}{\sqrt{x^2 + (a_o)^2}}\right)\right)}{4\pi\left(x^2 + \left(a_o - \sqrt{(r_c)^2 - x^2} + K\right)^2 + z^2\right)}, & convex \end{cases}$$

The convex and concave light intensity equations are used in the same manner as the light intensity for flat cells. The convex and concave intensity equations have been used in the bending experiments described in section 3.4.

3.3   Procedure For Applying Axial Stress

The MTS Universal Testing Machine was used to produce tensile stress of CIGS solar cell. The jaws of the MTS are only an inch wide, because the cell is ten inches wide this would result in on even stress distribution along the width of the cell. To create an even distribution of axial tensile stress on the cell, in-house clamping plates was fabricated. These custom clamping plates were created in Autodesk Inventor® and then 3D printed using Maker Bot+®.

A set of four plates were fastened to the solar cell, two at the top and two at the bottom. The plates were designed to cover the plastic material that the solar cells were embedded into while leaving the active area of the solar cells exposed. The plates were fastened on either side of the solar cells with a set of four screw, four nuts, and eight washers. The cell and plate assembly was then fastened into the jaws of the MTS Machine.

Figure 18: a) Set of 3D printed custom clamping plates designed to eliminate stressed concentrations within the solar cell. b) Experimental set-up

Once the CIGS cell is firmly placed on the universal testing machine, a series of tensile load is applied with 20lbf increment up to 100lbf. At every 20lbf increment, the machine was stopped and the electrical performance was collected with the solar analyzer.

The cell with its plastic incasing was found to have slight viscous-elastic properties, as such when the load was stopped there was some relaxation or relief of a small portion of load on the cell. To take this into account the load was set slightly higher than the target load and the average of the load ever a given period of set relaxation time was used. Relaxation time is defined as the period of resting time before applying the next increment of stress. The offset was always choses so the average value of stress came within a few tenths to the target stress.

To accomplish this, an in-house testing template was created for the MTS Elite® software. Once started the template would ask for the train rates in in/sec, as well as the target loads. Once these values were entered the MTS Machine would apply increasing load in a manner that kept the strain rate fixed to match the entered value. Once MTS Machine reached a target load it would pause and wait for the operator to click the continue icon. The amount of time the pause lasted was determined by the operator and used for the relaxation time and data collection of the cell. The time was kept with the use of a stopwatch. After the allotted time had passed the operator would click the continue icon and the MTS machine would continue its increase of load until it the next target load. This process of load application, pauses, and continued load application, was sustained until the last target load was meant. After that the MTS Machine returned back to initial conditions

and the data was exported for processing. This process was the repeated with several strain rates: 0.0001, 0.001, 0.01, and 0.1 in/sec. as well as several relaxation time: 10, 5, and 1 minute.

The electrical performance of the cell was measure using a solar analyzer consisted of: Open circuit voltage (V_{oc}), Short circuit current (I_{sc}), Efficiency (η), and Current-Voltage curve (IV curve). The tensile stress was obtained by dividing the tensile load by the cross-sectional area of the solar cell, which is 0.565 in^2. The applied average stress vs. strain curve is shown in Figure 19.
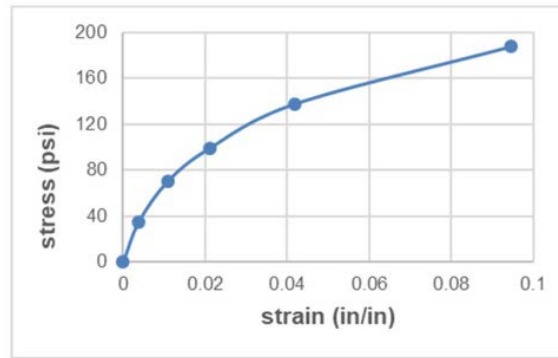
Figure 19: Stress vs. strain curve of CIGS solar cell

The same cell was used for each experiment. This caused degradation of the cell as illustrated in Figure 20. This degradation is identified by the negative slope of the trend line for the short circuit current and efficiency as the loading cycles increase. The open circuit voltage remains almost constant with a very slight increase as the loading cycles increase. The short circuit current and efficiency decreases as the loading cycles increases similar to the experimental results of Lee et al.[11]. To account for this degradation the ratio between the performance at give load (V_{oc}, I_{sc}, EFF), to the performance at zero load (Voc_0, Isc_0, EFF_0) is used to analyze the effect of stress at a given strain rate and relaxation time, instead of using the absolute value of performance of solar cells.
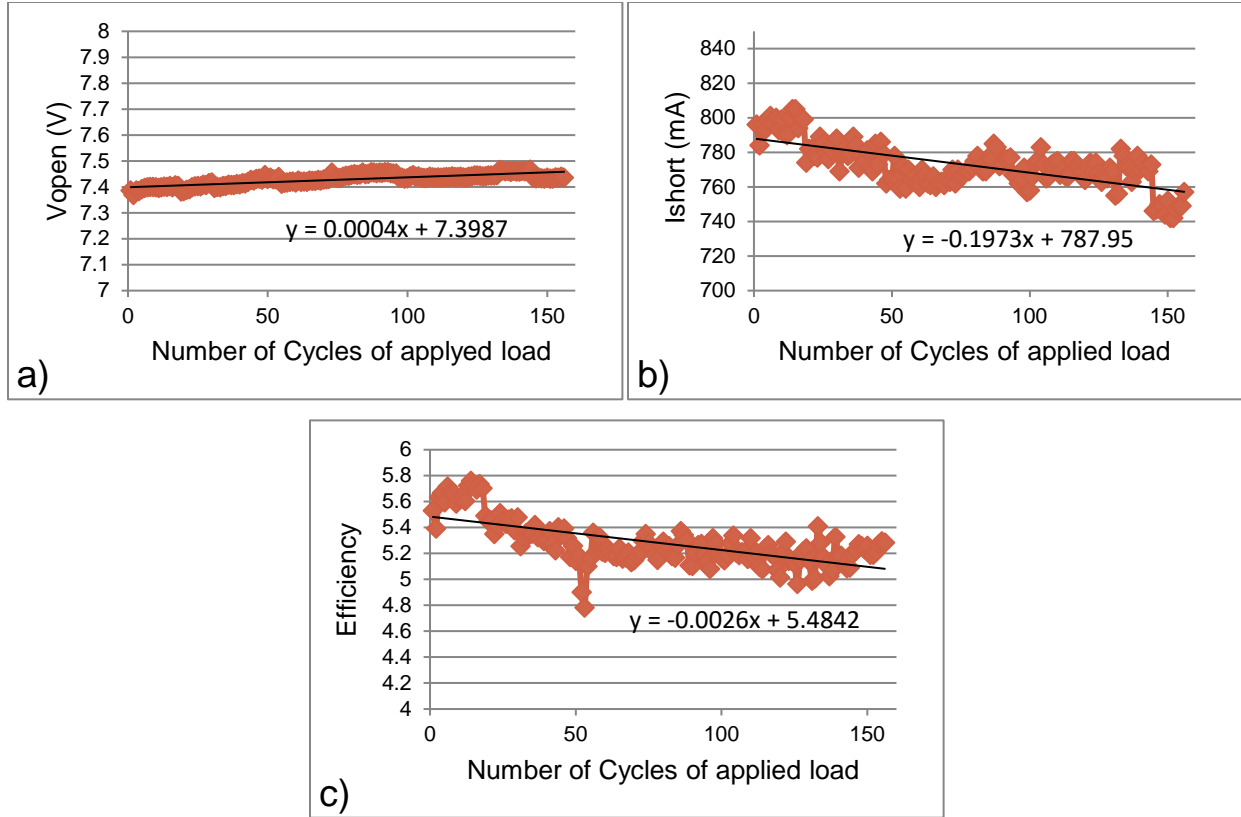
Figure 20: a) Open circuit voltage vs. Number cycles of applied load b) Short circuit current vs. Number cycles of applied load c) Efficiency vs Number cycles of applied load

3.4 Procedure For Bending Stress

This set of experiments consisted of collecting the solar cell parameters of V_{oc}, I_{sc}, P_{max}, EFF, and FF while the solar cell was bent into a concave or convex curve with a given radius r_c. To achieve these given radius several sets of solar cell braces were created in Autodesk Inventor®. Each set consisted of three braces with a given radius. Each piece had a convex and concave curve of identical radius. They were fabricated with 3D printing

Figure 21: A set of solar cell braces with radii of 0.082 m

A total of seven sets were made. Each set had a different radius. This allowed for various cell radii to be tested in both concave and convex.

Figure 22: All seven types of solar cell braces. Radii increase going from left to right

To set up the bending experiment start with slipping the solar cell into one of set of braces. The braces are designed to be located at the top, middle, and bottom of the cell to create a consistent curvature across the length of the cell.

Figure 23: Solar cell set inside of braces. One located at the top, middle, and bottom of the cell to keep uniform curvature.

Once the cell was in the braces it was propped up in the MTS clamps. The cell then underwent the standard light soaking procedures and collection of solar cell parameters as described earlier in section 3.1. Once the data was collected the cell was placed back in its box for exactly twenty four hours. This was done to allow any stress from being held in a curved form to relax out as well as to reset the residual current and voltage that had accumulated from the light soaking and data collection. This was repeated each day with a different radius for both concave curvature and convex curvature. The radii were chosen based on the depths of the arc depth the cell made.

Table 2: Cell depths and radii

D (in)	D (m)	r_c (in)	r_c (m)
2.21	0.056134	3.226202	0.081946
2	0.0508	3.69165	0.093768
1.75	0.04445	4.359272	0.110726
1.5	0.0381	5.206055	0.132234
1.25	0.03175	6.344105	0.16114
1	0.0254	8.007813	0.203398
0.5	0.0127	16.25	0.41275
0	0	inf	inf

3.5   Procedure For Applying Rolling Stress Induced Damage

Once the cell has completed its light soaking is complete, collect the base line sample of zero damage using the solar analyzer. Once the base line is collected remove the cell from the MTS machine that is used to prop it up. Insert the other side of the cell into the top jaws of the MTS machine and tighten the jaws. This process is to help you roll the cell around the dowels if there is no one to assist. Make sure the cell is held taught in a horizontal manner to make the rolling easier as shown in the figure 24. For the smaller diameter dowels an attached lever is used to assist in making and keeping a tight roll.
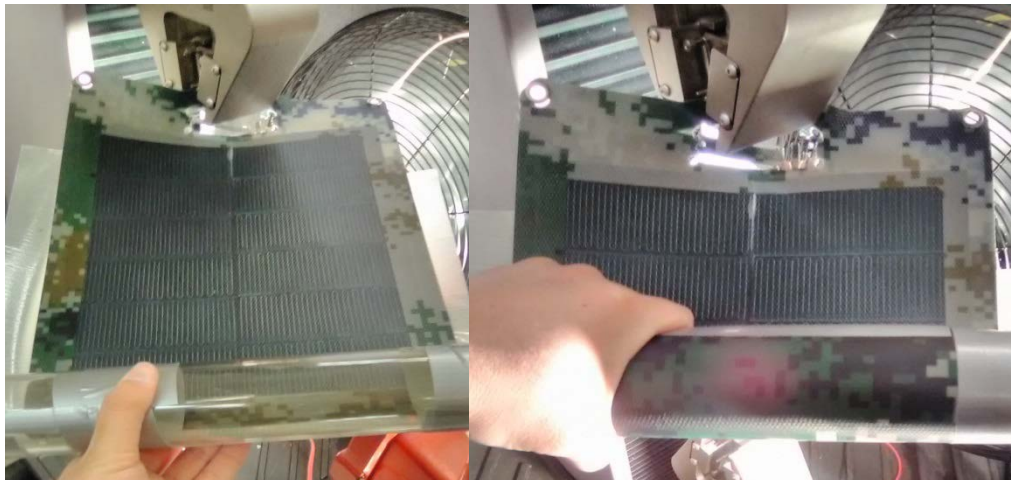
Figure 24: Left a 2 inch diameter dowel attached to the end of a solar cell. Right Solar cell partially rolled along the 2 inch dowel

After completely rolling the cell, hold the cell in the bending position for 1 minute. This time is kept using a stopwatch. The cell is held for one minute to allow the crystalline structure of the cell to adjust, realign and set in their new place in response to the large amounts of stress the rolling has created in it. After one minute, release and remove the tape and dowel from it. Secure the lower sell upright in bother of the MTS jaws and reattach the thermistor and solar analyzer leads. The lamp and the fan are still be in on and in their designated locations, once the cell is propped back up the measurements can be taken. This process was repeated with dowel diameters of 2, 1.75, 1.25, 1, 0.5, and 0.25 in. It was also done for to having the active layer of the cells in tensile stress, cell rolled towards the dowel, and compressive stress of the active layers, cell rolled away from dowel.

4. SIMULATION PROCEDURE

4.1   MatLab Simulation

The matlab script uses the data from the solar analyzer as well as temperature information to create a fit curve between the experimental data and the single diode model for a solar cell. This model characterizes the solar cell as a circuit that consists of a voltage source in parallel with a diode, I_d, a shunt resister, R_{sh}, and a series resister, R_s. the layout of the circuit can be seen in figure 25 below.
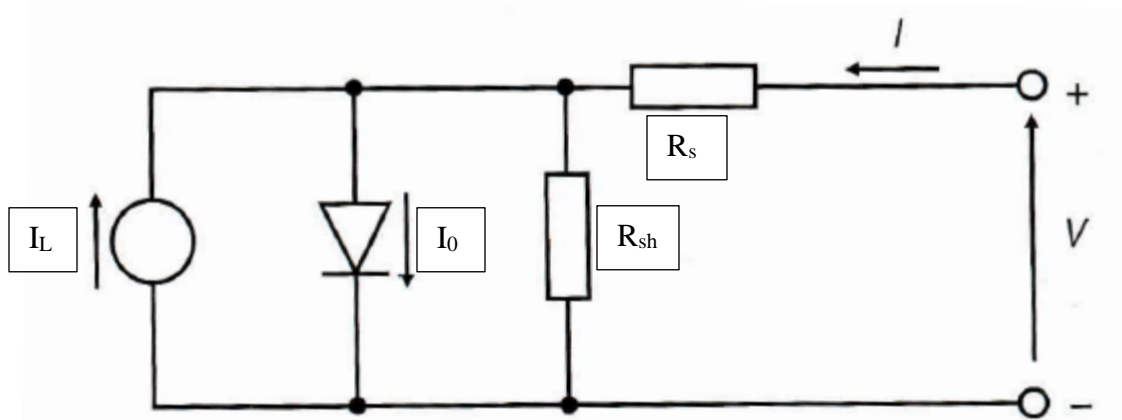
Figure 25: Diagram of the Single diode model of a solar cell [3]

4.1.1   Series and shunt resistance

This model is taking the established idea diode model of a solar cell and using the resistive terms to take into account real world defects that will reduce the cells performance. The first resistive term is the series resistance, R_s. This term represents the restive losses that accuses between layers of the active materials as well as at the junctions of the active layers to the metal contacts [27] . This resistance decreases the performance of the solar cell as it increases, bringing the cell further from the ideal diode.
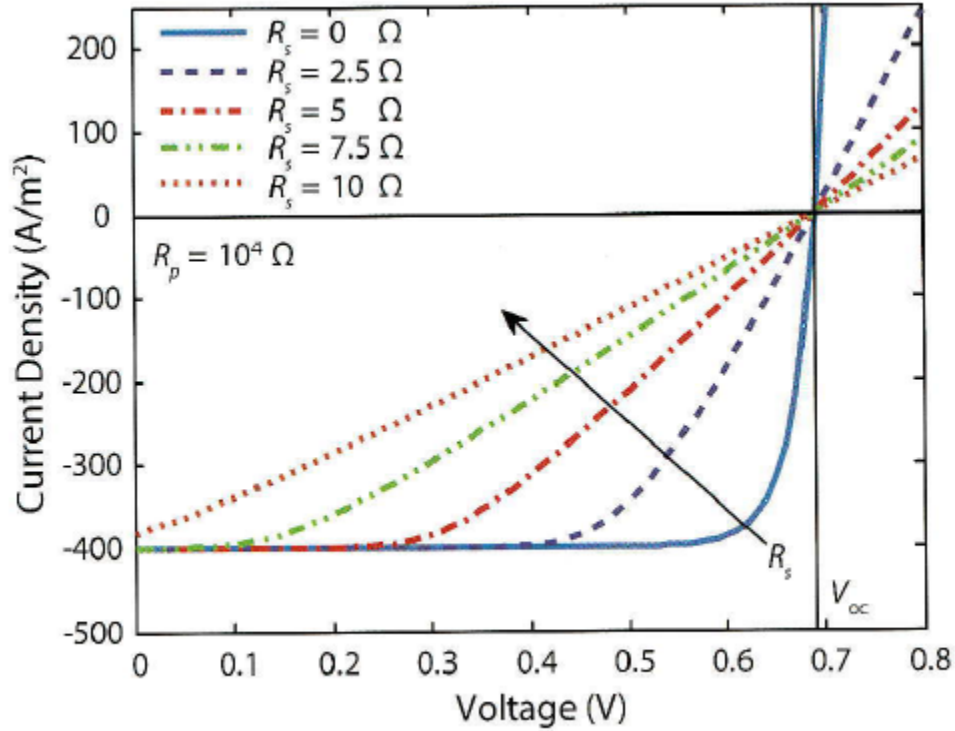
Figure 26: The effects of series resistance on a solar cell [3]

The second resistive turn is the shunt resistance. This term represents the resistive losses that come from manufacturing defects. These defects are located around the edges of the solar cell as those are areas where the crystalline structure abruptly stops [27]. This resistance is placed in series with the diode because it acts as an alternative route that current can flow through leaving the diode inactive. The lower the shunt resistance is the solar cell will behave less like an ideal diode. It is best to have a very large shunt resistance and a very small series resistance.
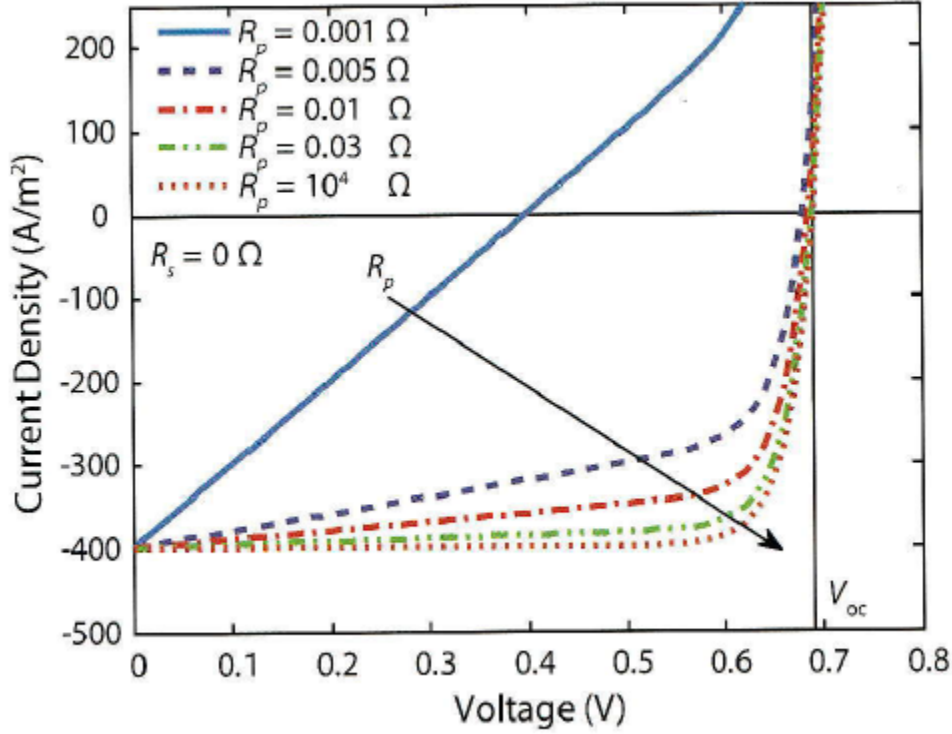
Figure 27: The effect of shunt resistance on solar cells [3]

4.1.2 Single diode equations and effects of dark and light current

Using the diagram for the single diode model and using kerchief's the current law current as a function of voltage can be found. The governing equation for this circuit is as follows:

$$I = I_L - I_0 \left(e^{\frac{q(V+IR_S)}{nk_bT}} - 1 \right) - \frac{V + IR_S}{R_{sh}}$$

Where, I is the output current, and n is the ideal diode factor, which has been set at 1.5 for this equation. This equation is a complex one as its output is dependent on itself. Normally this type of equation will require a recursive numerical method to solve/

The matlab script used takes the experimental current voltage curves and finds the parameters of I_L, I_0, R_s, and R_{sh} to find the best theoretical curve fit. A recursive numerical method is used in this script assist in finding these parameters

4.1.3 How the script works

The first 40 lines are used for collecting the raw data from the solar analyzer data file, assigning the date to appropriate vectors finding the thermal voltage and finally plotting the raw data. A good portion of those 40 lines are explanatory comments for the purpose of the lines of code. The next 25 lines of code to set initial values, for the minimize function called fminsearch, which calls a custom function and finally assigns the resultant vector to individual variable [29].

The second files is the custom function that us called within the minimize function. The 19 lines of this function accepts the inputs from the minimizes function as well as the raw data values of diode ideality factor n, thermal voltge Vt, and initial temperature T1, along with the raw data vectors of curr for current, and volt for the voltage. It then uses a "for loop" to fill a blank vector with a vpsolve solution for each of the data point in the volt vector. Once that vector is filled it takes the difference between the data in curr vector and the filled y vector and assigns the difference to the vector f. Vector f is then normalized and returned to the minimizing function.

The minimize function then uses the normalized f value to adjust the initial parameters of IL, I0, Rs, and Rsh then feeds them back into the custom function. The processes is then repeated until the minimizing function finds the smallest normalized value of vector f, and it's associated inputs of IL, I0, Rs, and Rsh.

According to matlab the fminsearch function, looks for a local minimum at a point x, described by the function f, where x is an input vector or input matrix and f is the output function which produces a scalar value.

$$\text{fminsearch} = \min_x f$$

In essence the fminsearch for this script is finding the local minimum for a four dimensional function of IL, I0, Rs, and Rsh.

Because the fminsearch is finding a local minimum the input values are very important as the function looks for the closest minimum to that point described by your initial guess values.

The light saturation current, IL, is assumed to be equal to the short circuit current as it is in the ideal case when the. The dark circuit current, I0, is given for the ideal case at the open circuit voltage, given by

$$I0 = \frac{IL}{(e^{-\left(\frac{qV_{oc}}{k_bT}\right)} - 1)}$$

The series resistance, Rs, can be roughly found as the inverse slope to the current-voltage [27] curve at the open circuit voltage. The shunt resistance can be approximated as the inverse slope to the current-voltage curve at the short circuit values [27]. Taking the derivatives or the single diode equation at those points would show the values, it the other parameters were known. Because none of the parameters are known for these initial guesses the inverse slopes are found from the data using.

$$m_{inverse} = \left(\frac{y_2 - y_1}{x_2 - x_1}\right)^{-1}$$

With these as the initial values a rough estimate of where the local minimum is can be passed to the fminsearch function and the parameters can be found. This single diode model was used to evaluate the detrition of the solar cells used in the rolling experiments. These results are discussed later in chapter five.

4.2   COMSOL Parameter Values Simulation

A 3D model template of the three active layers of a CIGS solar cell was used to examine the theoretical limits of the of CIGS solar cell parameters as specific material properties were varied for extreme cases. This template was designed by a previous research done at Purdue University Northwest. The model makes use of the COMSOL MultiPhysics software and its pre-installed semiconductor physics module.

The template uses the material properties, ambient temperature, illumination, model dimensions, and applied voltage as impute parameters. The model consists of three layers, A zinc Oxide top layer, a cadmium sulfide layer, and a copper indium gallium diselenide layer as seen in the figure 28 below.
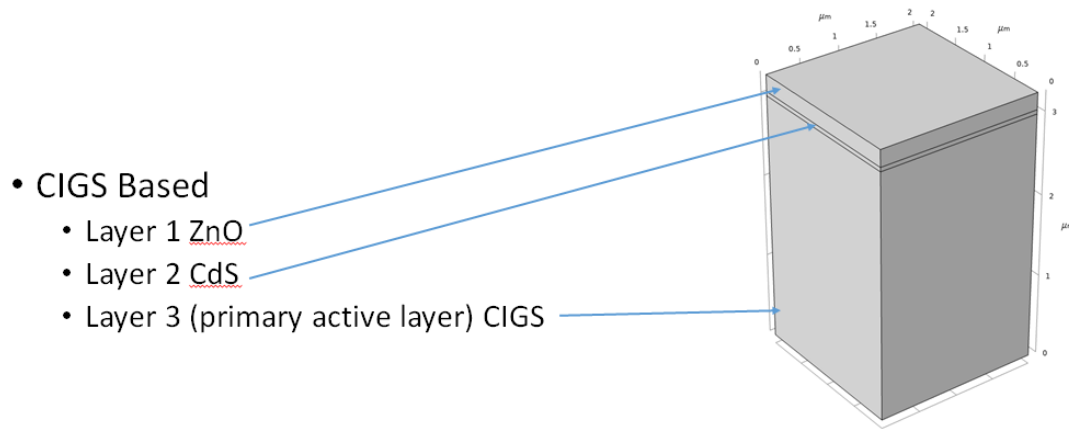
Figure 28: Diagram of CIGS Solar cell modeled in COMSOL Multiphysics

All three of these are active layers have their material properties added. These material properties include: Layer Thickness, Relative permittivity, Electron and Hole mobility, Band-gap, Effective density of states for the conduction and valence band, Electron affinity, Electron and hole Carrier density, hole and electron life time as well as the number of traps and intrinsic carrier concentration.

The software includes the Shockley-Read-Hall recombination and regeneration to take into account losses of charge carriers within the bulk of the material. To properly analyze the properties of the midgap defects states are provided for each material. These include Defect density for acceptors and donors and the Capture cross section for wholes and electrons. To take into account losses at the contacts the Schottky contact properties were added for each material, which are the surface recombination velocity for holes and electrons.

Finally the environmental properties were added to the model [29]. These environmental properties were the input power density, temperature, and an applied voltage range. The voltage range is added is a parametric study variable. The base line material properties, the properties that were identified by Gloeckler et al. [30] for recombination as well as the environmental parameters listed in the table 3 below.

Table 3: CIGS solar cell baseline parameters

Layer properties			
Layer	Zn0	CdS	CIGS
Thickness (nm)	200	50	3000
Relative permittivity, ε	9	10	13.6
Electron mobility, μ_n (cm^2/Vs)	100	100	100
Hole mobility, μ_p (cm^2/Vs)	25	25	25
Band-gap,E_g (eV)	3.3	2.4	1.15
Effective density of states, $N_c$conduction band(cm^-3)	2.2×10^{18}	2.2×10^{18}	2.2×10^{18}
Effective density of states, $N_V$valance band(cm-3)	1.8×10^{19}	1.8×10^{19}	1.8×10^{19}
Electron affinity, χ_e (eV)	4.4	4.2	4.5
Carrier density , (cm^-3)	$N_D: 10^{18}$	$N_D: 10^{17}$	$N_A: 2 \times 10^{16}$
Gaussian (midgap) Defect States			
Defect density, $E_{A/D}$(cm^-3)	$D: 10^{16}$	$A: 10^{16}$	$D: 10^{12}$
Capture cross section, σ_n	10^{-12}	10^{-17}	5×10^{-13}
Capture cross section, σ_p	10^{-15}	10^{-12}	1×10^{-15}

Schottky contact properties		
	Front contact	Back contact
Surface recombination velocity, electrons: S_e(cm/s)	10^7	10^7
Surface recombination velocity, holes: S_p(cm/s)	10^7	10^7
Metal work function, ψ (eV)	4.45	5.45
Non-material parameters		
Ambient temperature (C^0)	25	
Light source (W/m$^{2)}$	1000	
Applied voltage range (V)	0-0.7 or 0-0.8	0.01 step

With these properties the software will use a finite element analysis to solve the poisons, continuity, and transport equations, as well as the Shockley Read Hall equations to create a single current-voltage curve shown in figure 29.
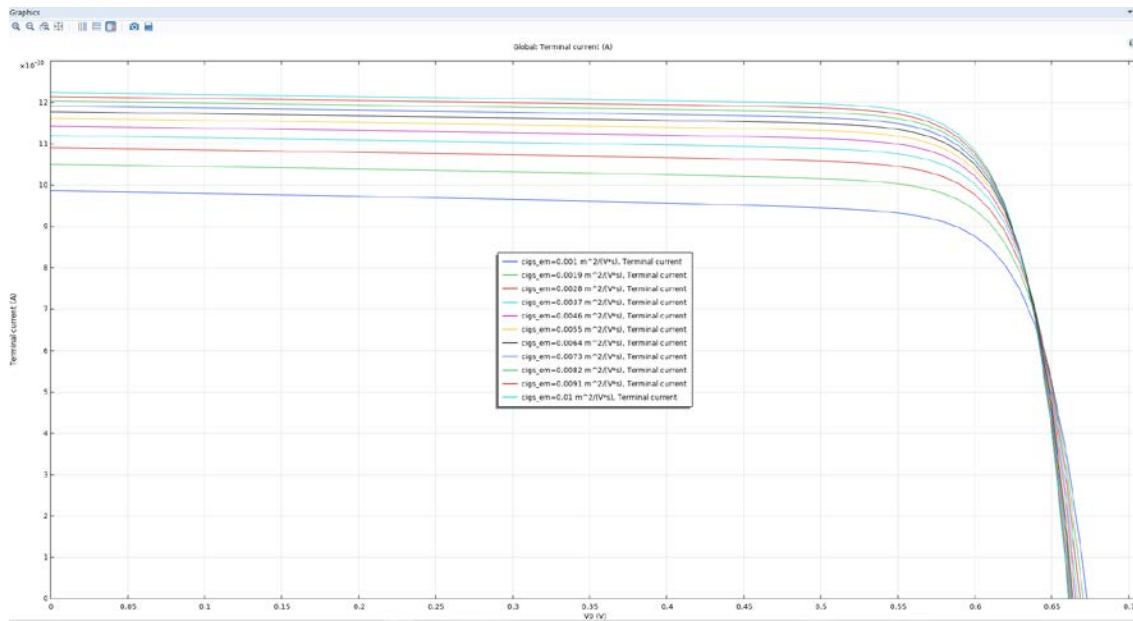

Figure 29: A set of I-V curves created in COMSOL Multiphysics for the hole life time.

As seen in the plots above there are several current voltage curves plotted. This is the result of adding a second parametric variable. It is this second variable that is being studied with these

simulations. Four different simulations were done each with a different second parametric variable. Each simulation used one of the material properties for the active CIGS layer, they were the electron mobility, electron life time, hole mobility, and hole life time. For each simulation only one of the CIGS material properties were varied while there other three were held at their standard values. The four simulations were run multiple times with various ranges to obtain trend in the open circuit voltage, short circuit current, maximum power, efficiency, and fill factor. How the change in material property effects the before listed solar cell properties are discussed in chapter five. A table of the ranges for each material property is listed below.

Table 4: Ranges used for each run of the parametric study

property	Range 1		Range 2		Range 3		Range 4		Range 5	
EL	1E-10	4E-09	1E-10	1E-07	4E-15	4E-12				
EM	80	120	0.001	200.001	0.001	1000	300	1000	0.0001	0.1
HL	1E-07	4E-06	1E-07	9.1E-06	1E-09	0.0001	0.00001	0.000193	1E-12	1E-09
HM	5E+00	45	0.001	200.001	0.0001	100	0.0001	0.1		

5. RESULTS AND DISCUSSION

5.1 Results Of Tensile Experiments And Discussion

Due to large fluctuations caused by experimental uncertainties it is not possible to find any definite trends that can be applied to every case but some general trends can be found in most of the cases. Moreover due to these fluctuations in data, it was not possible to draw any conclusions for the maximum power, efficiency, or fill factor from these experiments.

Figure 30 shows the effect of axial tensile stress of the open circuit voltage ratio (Voc/ Voc) one can find two trends that apply to most cases. The first is that open circuit voltage increases slightly with increasing stress. The second is the rate of increase (the slope) increases with longer relaxation times.
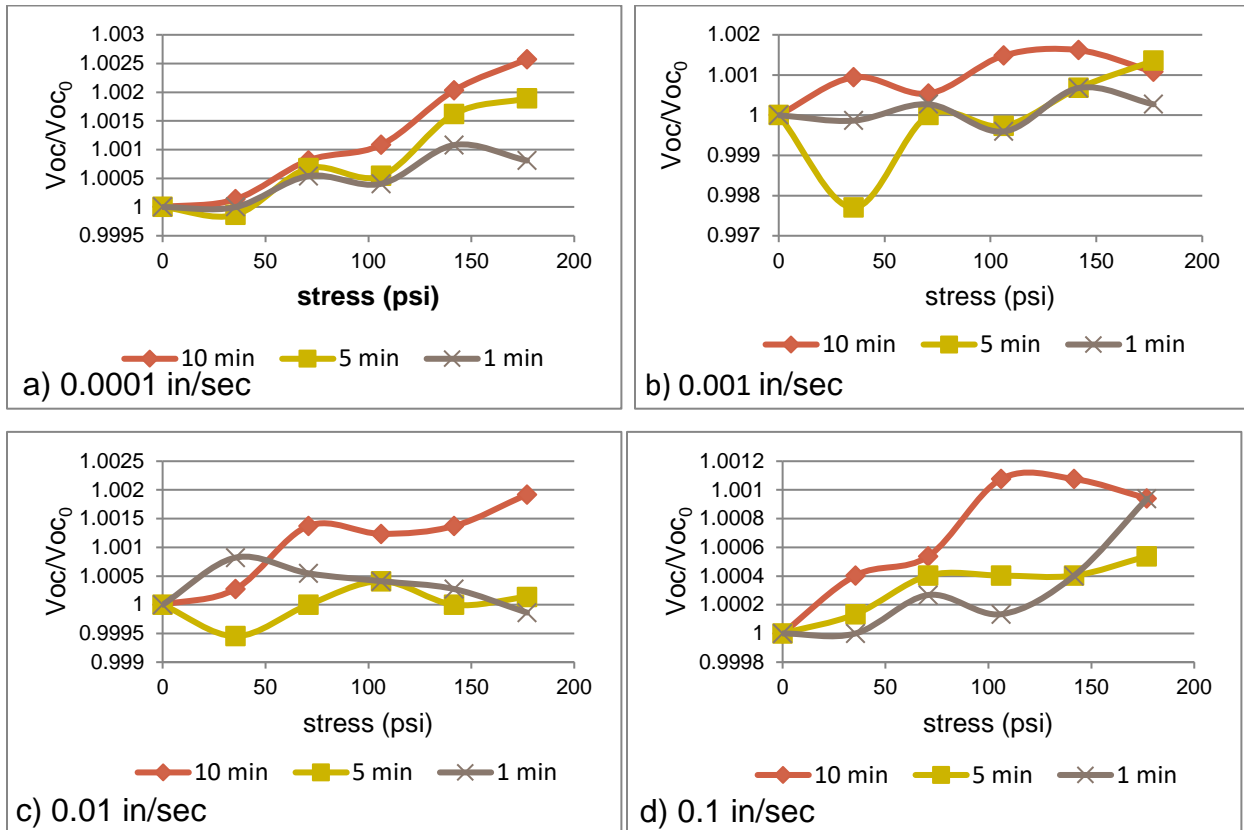

Figure 30: Note Orange is 10 minute relaxation, Yellow is 5 minute relaxation, brown is 1 minute relaxation time. (a) Voltage vs. stress with load application rate of 0.0001 in/sec (b) Voltage vs. stress with load application rate of 0.001 in/sec (c) Voltage vs. stress with load application rate of 0.01 in/sec (d) Voltage vs. stress with load application rate of 0.1 in/sec

Figure 31 shows the effect of axial tensile stress of the short circuit current ratio (Isc/I_{sco}) one can find two trends that apply to most cases. The first is that short circuit current generally is larger with larger stress. The second is there seems to be a general increase in the I_{sc} up to a given threshold of stress. After that threshold the I_{sc} seems to decrease. The threshold stress varies depending on strain rate and relaxation time.
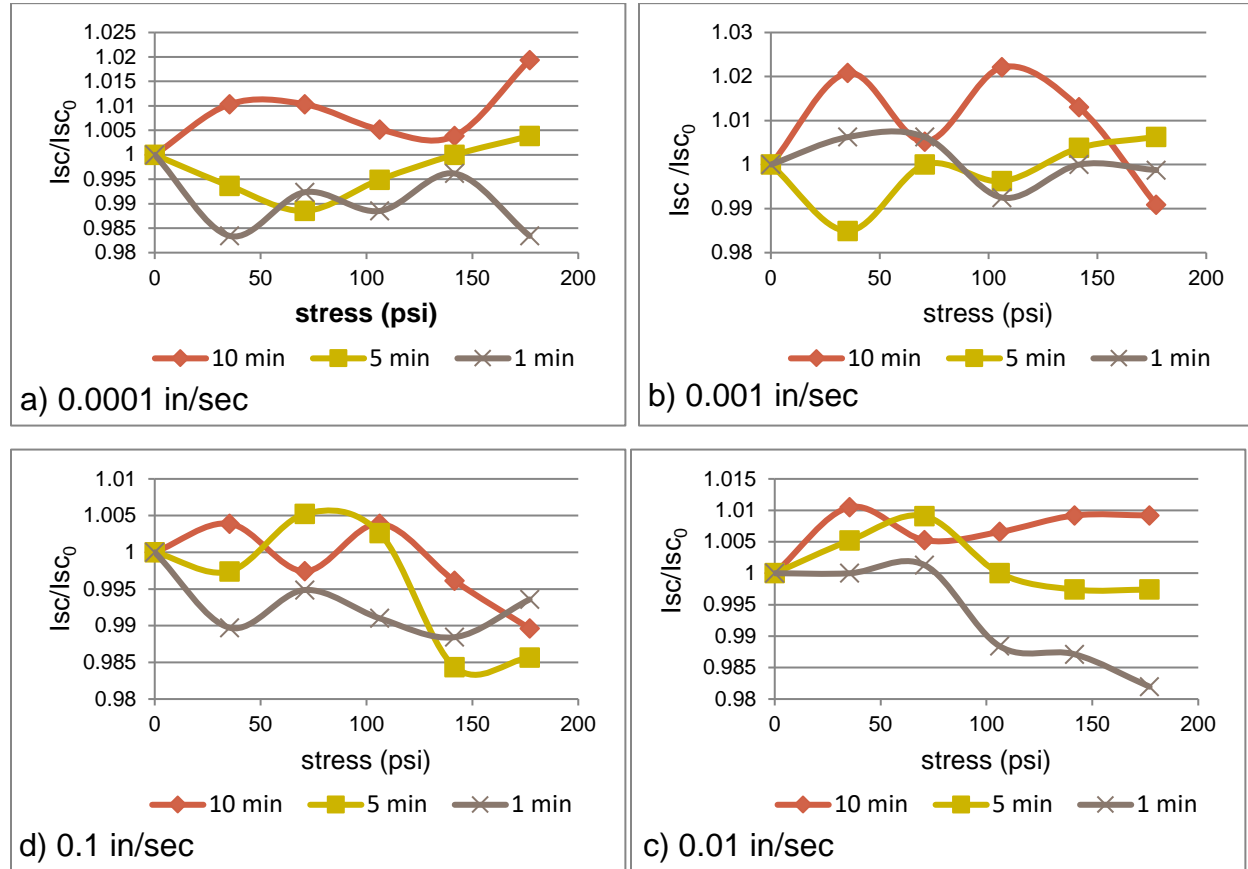

Figure 31: Note Orange is 10 minute relaxation, Yellow is 5 minute relaxation, brown is 1 minute relaxation time. (a) Isc vs. stress with a strain rate of 0.0001 in/sec (b) Isc vs. stress with a strain rate of 0.001in/sec (c) Isc vs. stress with a strain rate of 0.01 in/sec (d) Isc vs. stress with a strain rate of 0.1 in/sec

5.2   Results Of Bending Experiments And Discussion

Figure 32 displays the results of the bending experiments. There was a very slight if nonexistent downward trend for the open circuit voltage. The other parameters, short circuit, max

power, efficiency, and fill factor, all show clear but small downward trends with the cell bent towards the light source in a concave manor having a larger rate (slope) of decrease. It is not clear though if this is the result of stress or the gradient of the light source across the cell. This reduction in performance is believed to be the result of the active layer being place in compressive stress when set in a convex position but in tensile stress in concave position. This supports previously published work that compressive stress is more damaging than tensile stress.
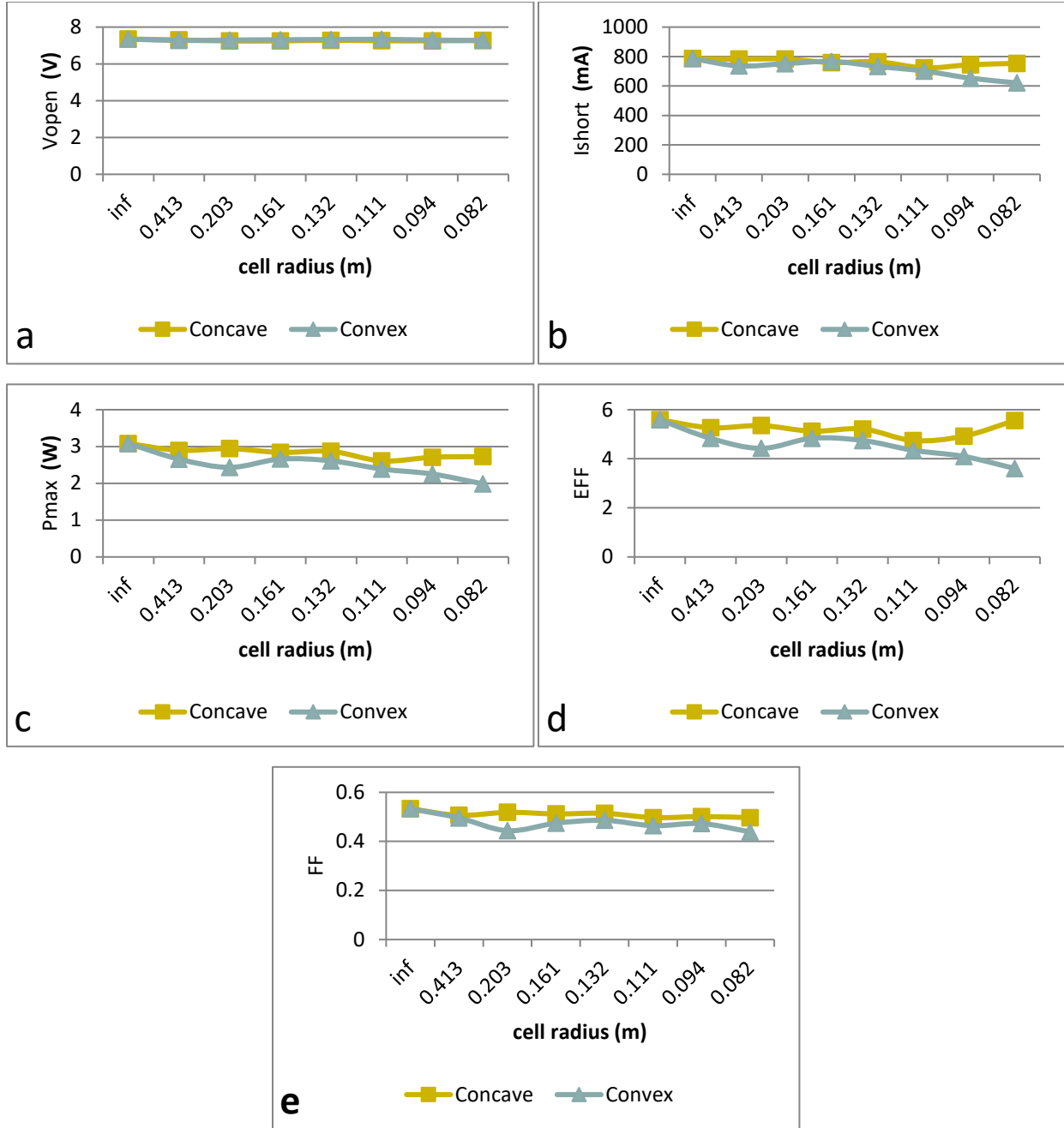
Figure 32: Plots for the V_{oc}, I_{sc}, P_{max}, EFF, FF as functions of cell radius and whether it's in a concave or convex position.

5.3   Results Of Rolling Experiments And Discussion

Figure 33 shoes the results of the rolling experiments and how decreasing dowel diameter affects the V_{oc}, I_{sc}, P_{max}, Eff, and FF. From these one can find three main trends. The first is that

rolling where the cells are facing away from the dowel creates more damage than rolling with the cell facing the dowels. This is because the active layer is in compressive stress when rolled with the cells facing away from the dowel. The second is there is a large drop in all solar cell parameters. For the V_{oc} this threshold diameter is one in but for the I_{sc} this diameter is 1.75 in. the remaining parameters decline around 2in. A third trend is that the P_{max}, EFF, and FF match closely with the I_{sc}. This means that the reduction of I_{sc} plays a large role in the reduction of performance than that of the V_{oc} when undergoing rolling damage. The existence of the threshold diameter and that compressive damage causes higher performance reductions are consistent with already published results. These results are also in agreement with the bending stress results.
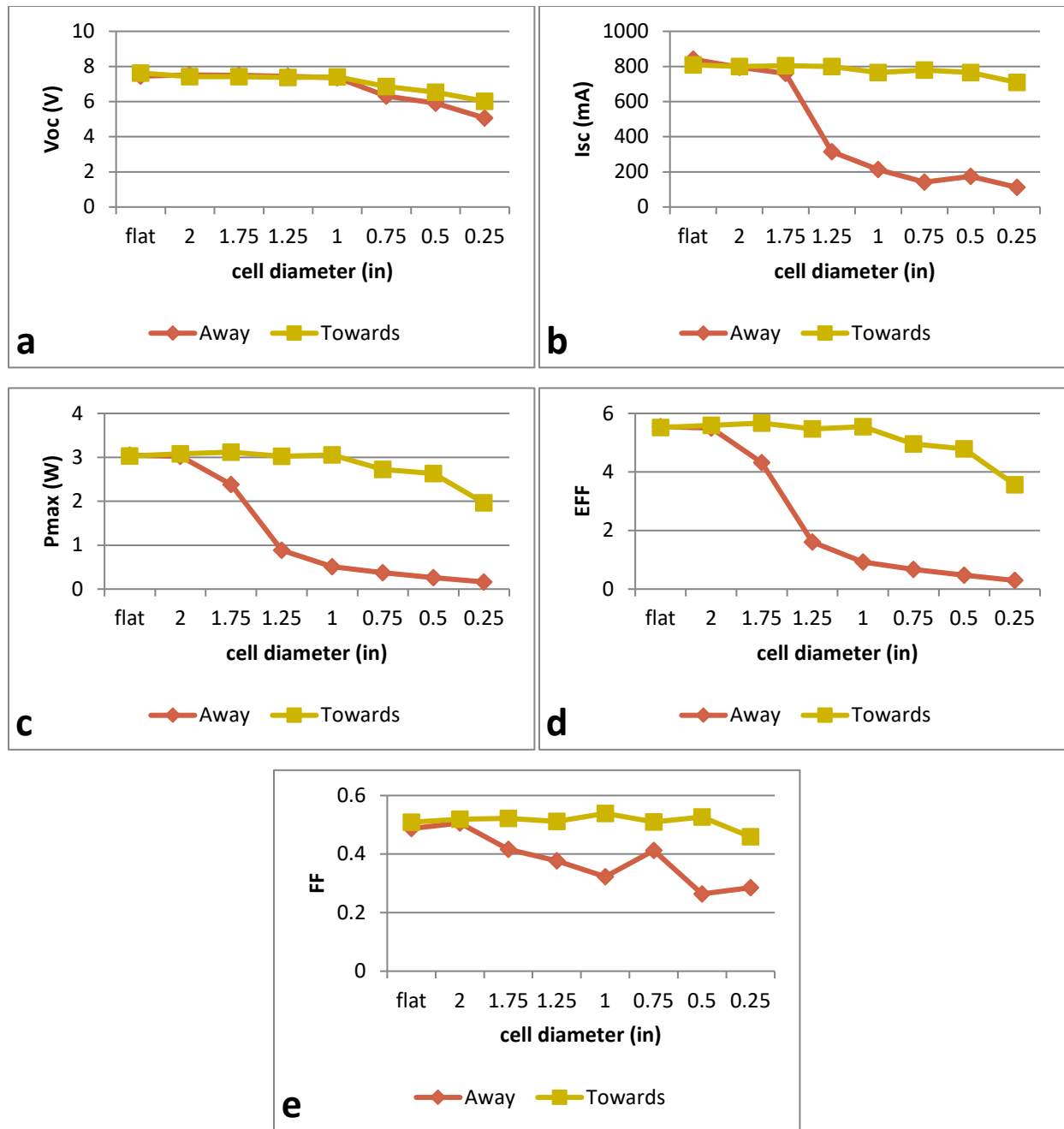
Figure 33: Plots for the V_{oc}, I_{sc}, P_{max}, EFF, FF as functions of dowel diameter and whether it's in a concave or convex position.

5.3.1 Matlab results

Figure 34 displays the results of the matlab analysis of the rolling data for rolling both cells towards the dowel and cells away from the dowel. The first trend is that for the series resistance

shows that the cells facing away from the dowel has a large increase as the dowel diameter decreases after 2in. While the series resistance for the cell facing towards the dowel for the most part is constant or very slightly increases. There are a lot of fluctuations in the shunt resistance results for both cells towards and away from the dowels but it seems as a whole the values seem to fluctuate around a constant value. The dark diode current is constant for both types of rolling but after dowel diameter reduces below 1in both increase with the cell towards the dowel having a much larger increase than the cell away from the the dowel. The saturation current for the cells towards the dowel has a slight downward trend to it while the cells away from the dowel has a large drop in saturation current for diameters smaller than 2 in.
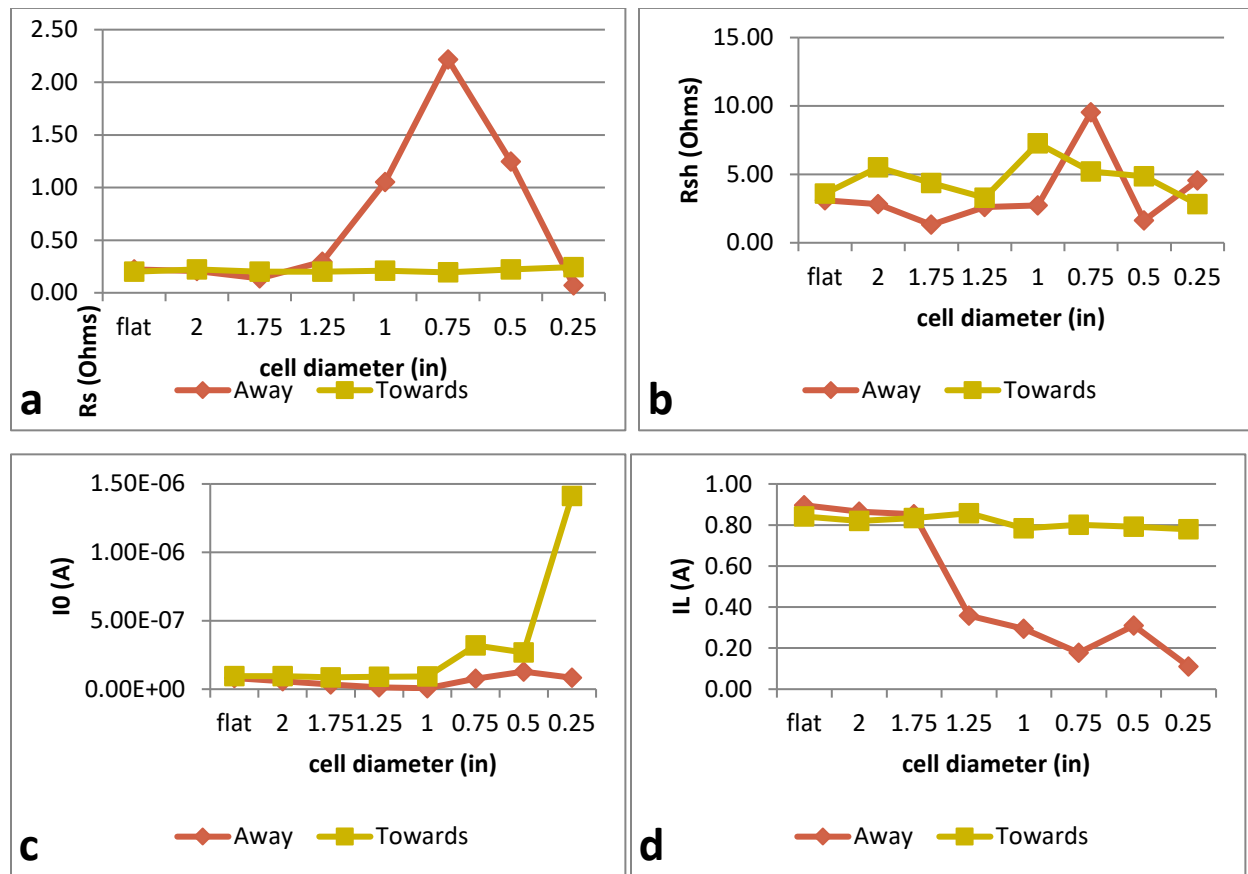

Figure 34: Plots for the R_s, R_{sh}, I_0, IL as functions of dowel diameter and whether it's in a concave or convex position.

The increase in the dark current and the series resistance as well as the decrease in the saturation current agree with the results of the solar cell parameters and the bending experiments.

Moreover the trend of the saturation current reduction matches those of the short circuit current from the solar cell parameters. This indicates the reduction of saturation current is the leading cause of deterioration in the solar cells.

5.4   Comsol Results Of Parametric Study

For the most of the results for the parametric study show that the solar cell properties of V_{oc}, I_{sc}, P_{max}, Eff, and FF, is an exponential manner that converges to a given value. This is consistent across all for material properties, EL, EM, HL, and HM that were varied in each of the studies. But when EL, EM, HL are very small, on the order of 10^{-4} times smaller than their accepted values, show a unique transient like responses. These responses are discussed below with the transient responses shown as inlays within the main plots.

5.4.1   Electron mobility

Figure 35 displays the effect of electron mobility on open circuit voltage. It depicts a decreasing exponential that levels off at 0.5 volts. In a range that four orders of magnitude smaller than the transient response is a small linearly decreasing trend. Figure 36 displays the effects of electron mobility on short circuit current, which shows an increasing exponential trend that levels off around 1.6 x 10^{-9} Amps. The transient region shows a small secondary exponential that levels off at 1.5x10^{-4} Amps before merging into the primary exponential. Figure 37 through figure 39 shows the maximum power, efficiency, and fill factor respectively all share the same trend. Each levels off at given value but shows a spike in the transient region that quickly tapers off to their respective given values.
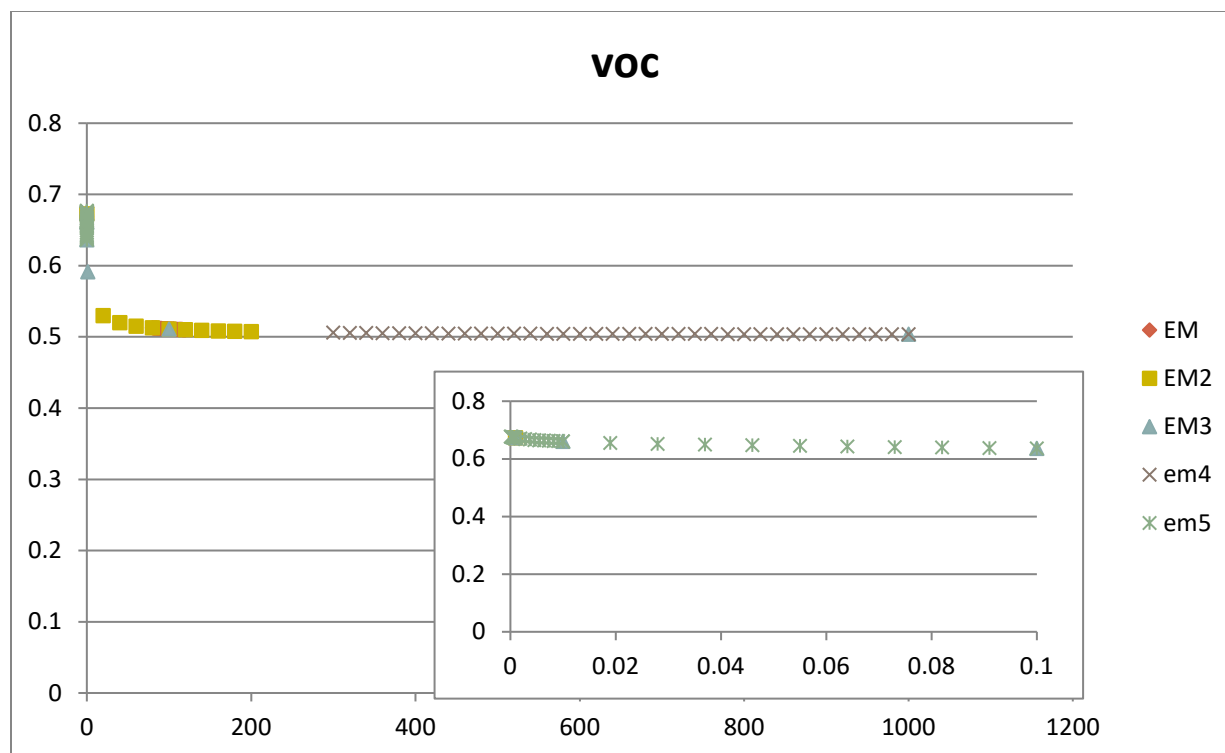
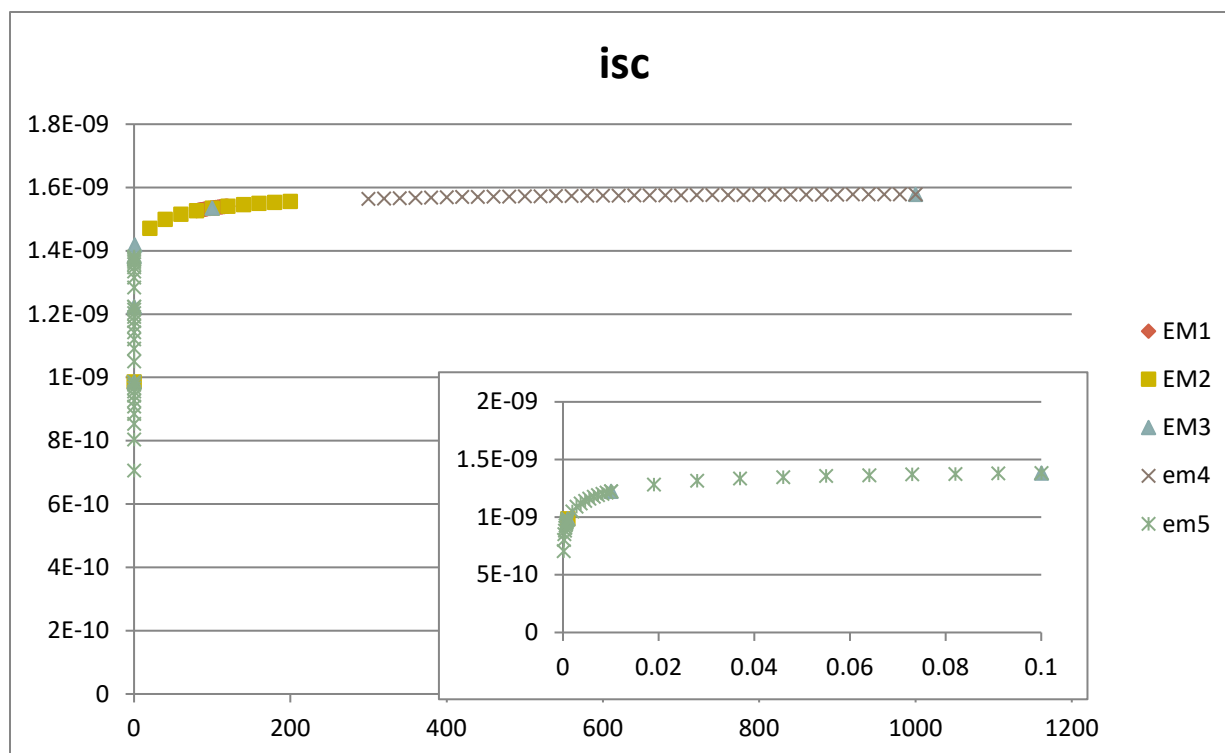Figure 35: V_{OC} as a function of electron mobility

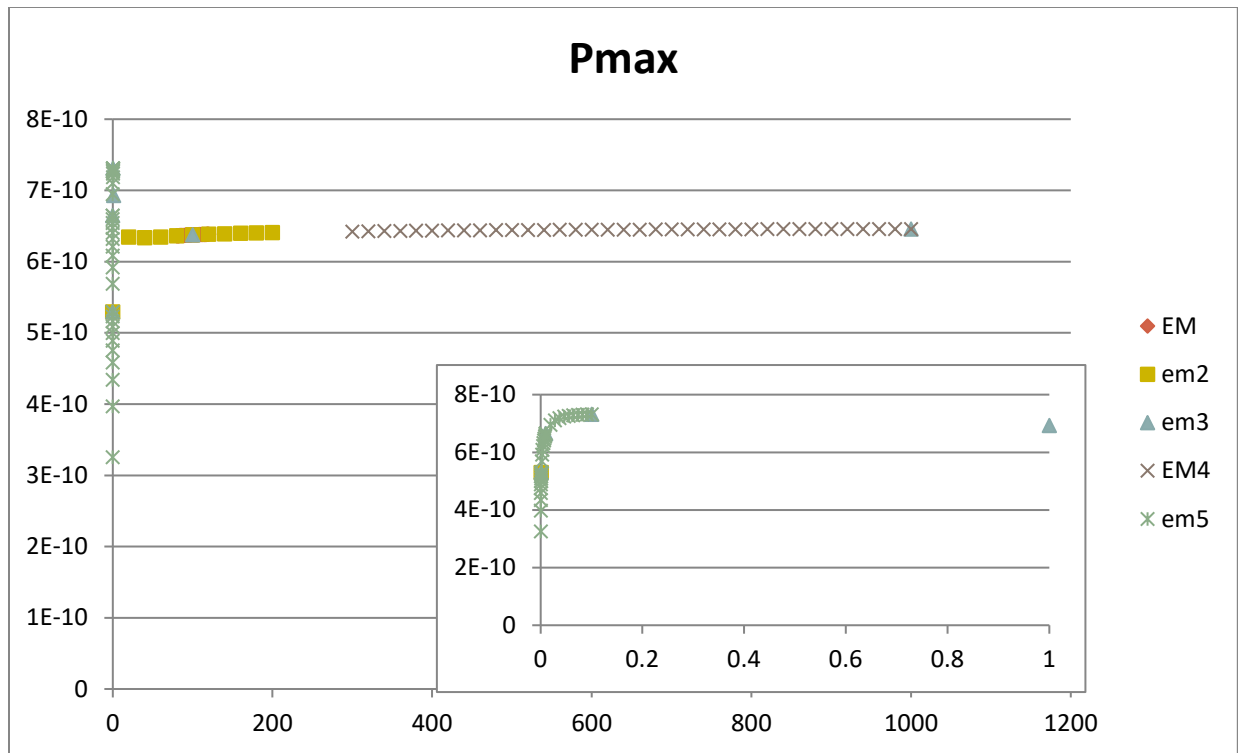Figure 36: I_{sC} as a function of electron mobility

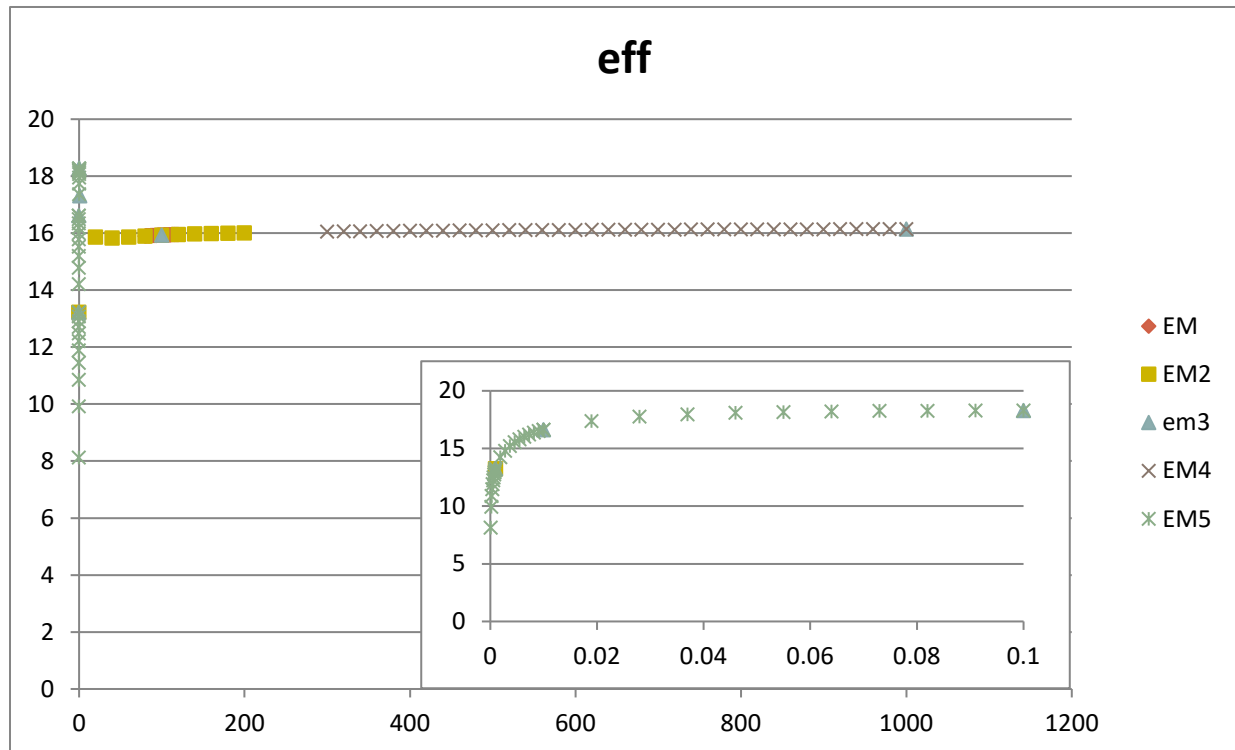Figure 37: P_{max} as a function of electron mobility

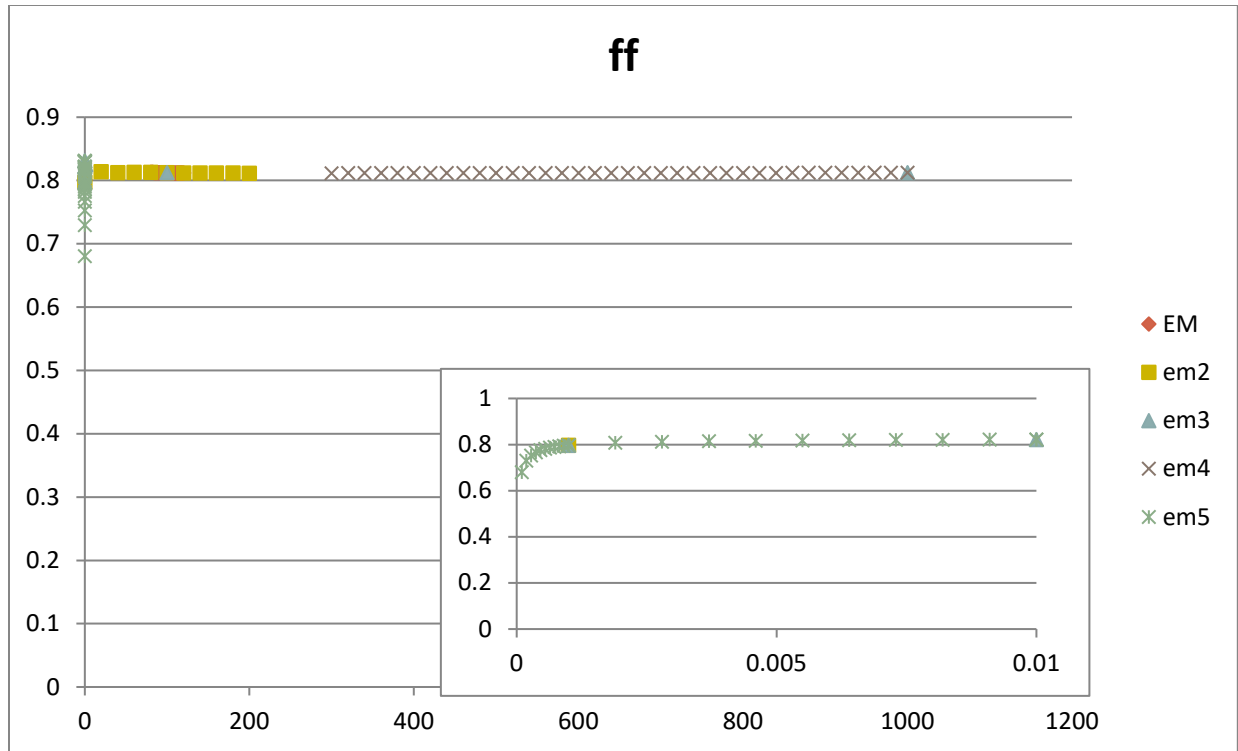Figure 38: EFF as a function of electron mobility

Figure 39: FF as a function of electron mobility

5.4.2 Electron life time

Figures 40 through 44 show the effect of electron life time on solar cell parameters of V_{oc}, I_{sc}, P_{mav}, EFF, and FF respectively. All display the same trend of an exponential increase and leveling off at a given value. All parameters also display the same transient response where there is a spike and small plateau before drastically dropping off and starting the exponential trend.
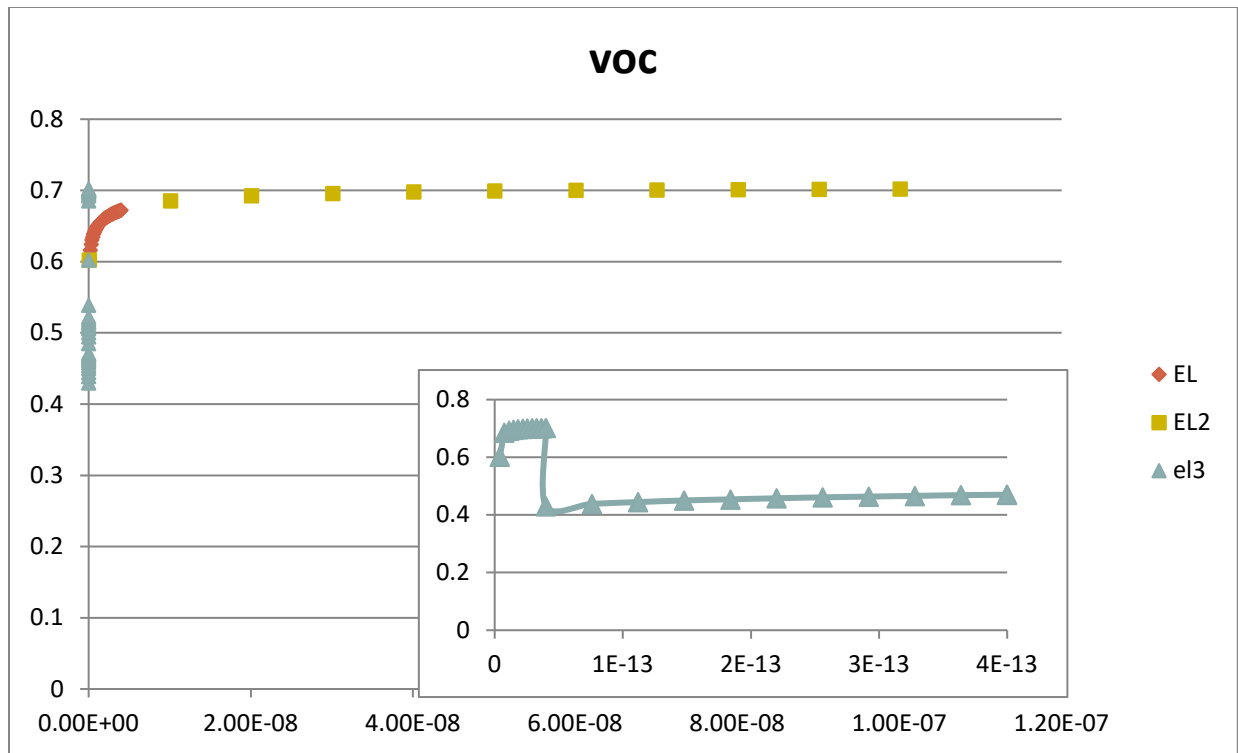
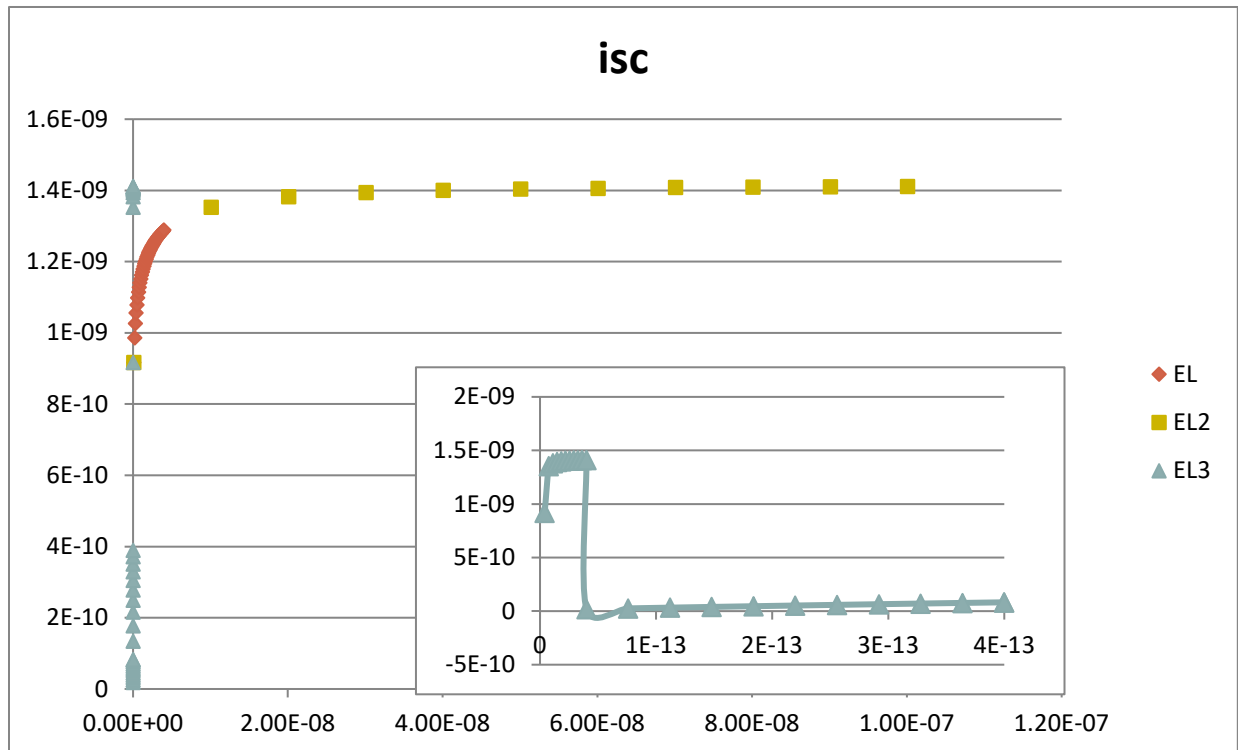Figure 40: V_{OC} as a function of electron life time

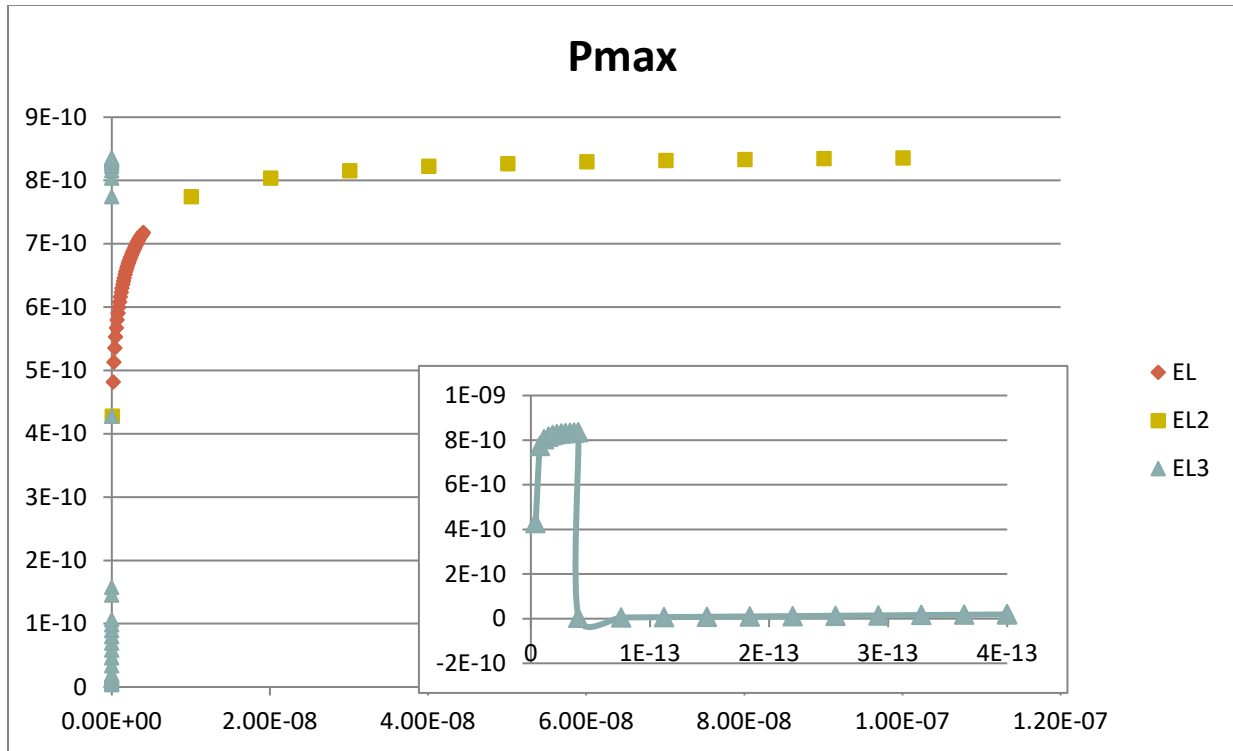Figure 41: I_{sC} as a function of electron life time

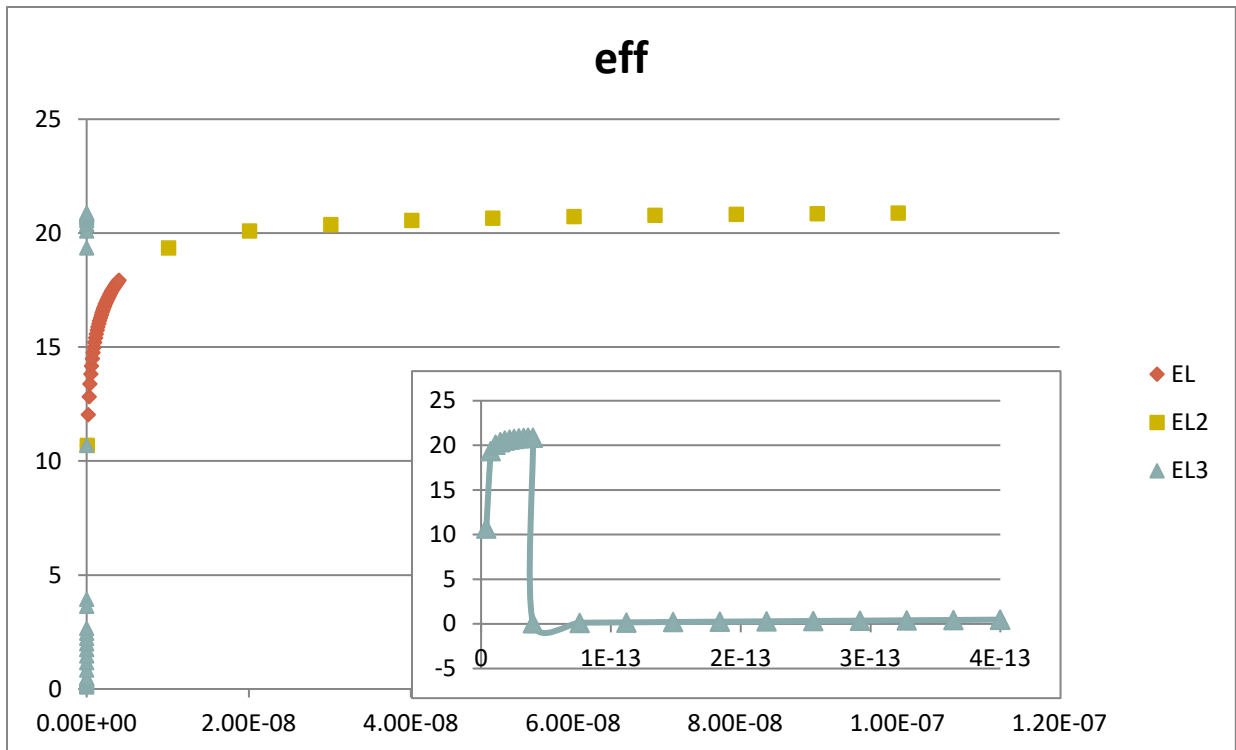Figure 42: P$_{max}$ as a function of electron life time

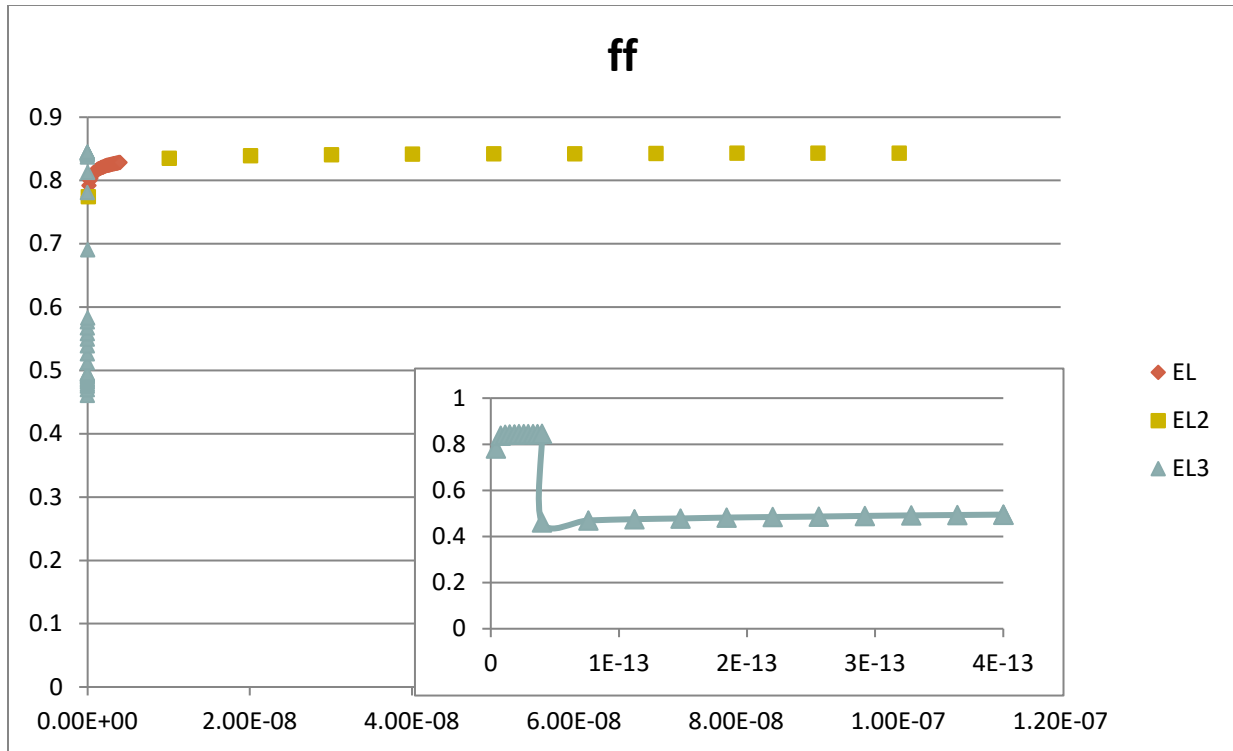Figure 43: EFF as a function of electron life time

Figure 44: FF as a function of electron life time

5.4.3 Hole mobility

Figure 45 displays the effect of hole mobility on open circuit voltage. It depicts an increasing exponential that levels off at 0.660725 volts. The transient range is a small oscillating spike which drops off into the exponential trend. Figure 46 displays the effects of hole mobility on short circuit current, which shows an "L" shape to it which remains fairly constant around 1.22 x 10^{-9} Amps. The transient region shows a small decaying exponential. Figure 47 through figure 49 shows the maximum power, efficiency, and fill factor respectively all share the same trend. Each levels off at given value by an exponential trend but each also shows a spike that has slight oscillations in it before transient region that quickly tapers off to their respective given values.
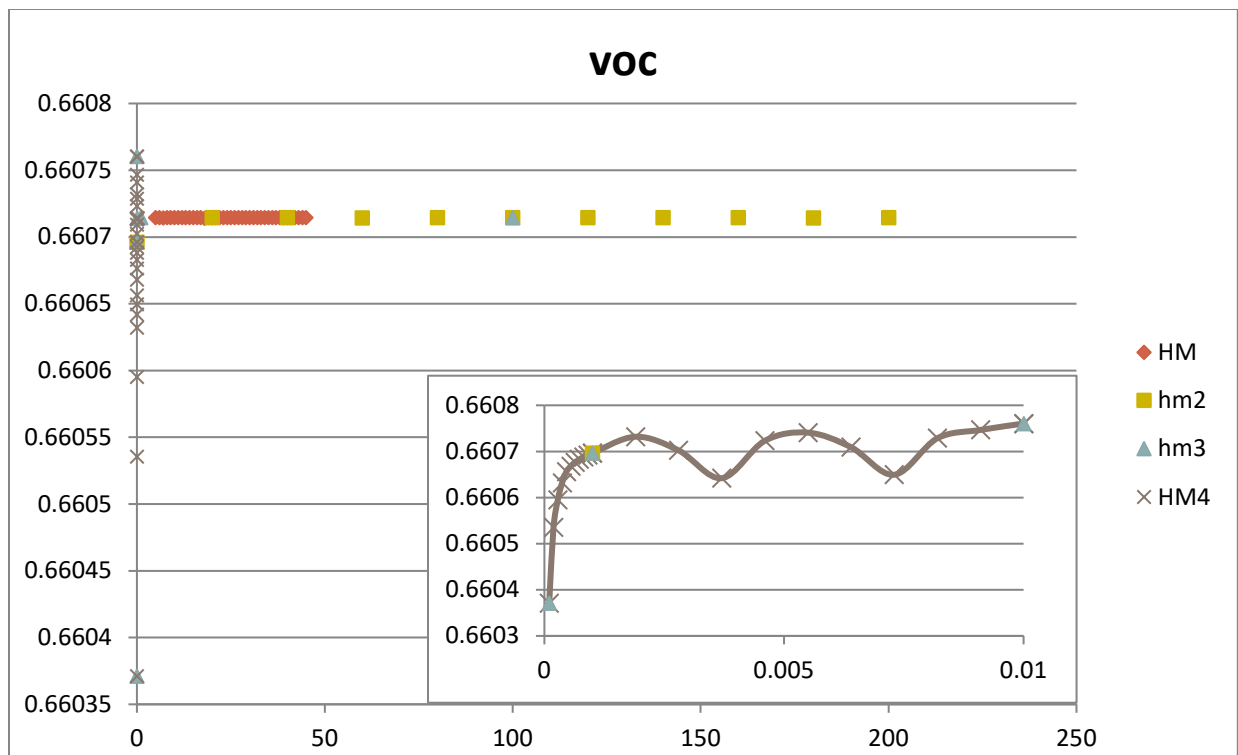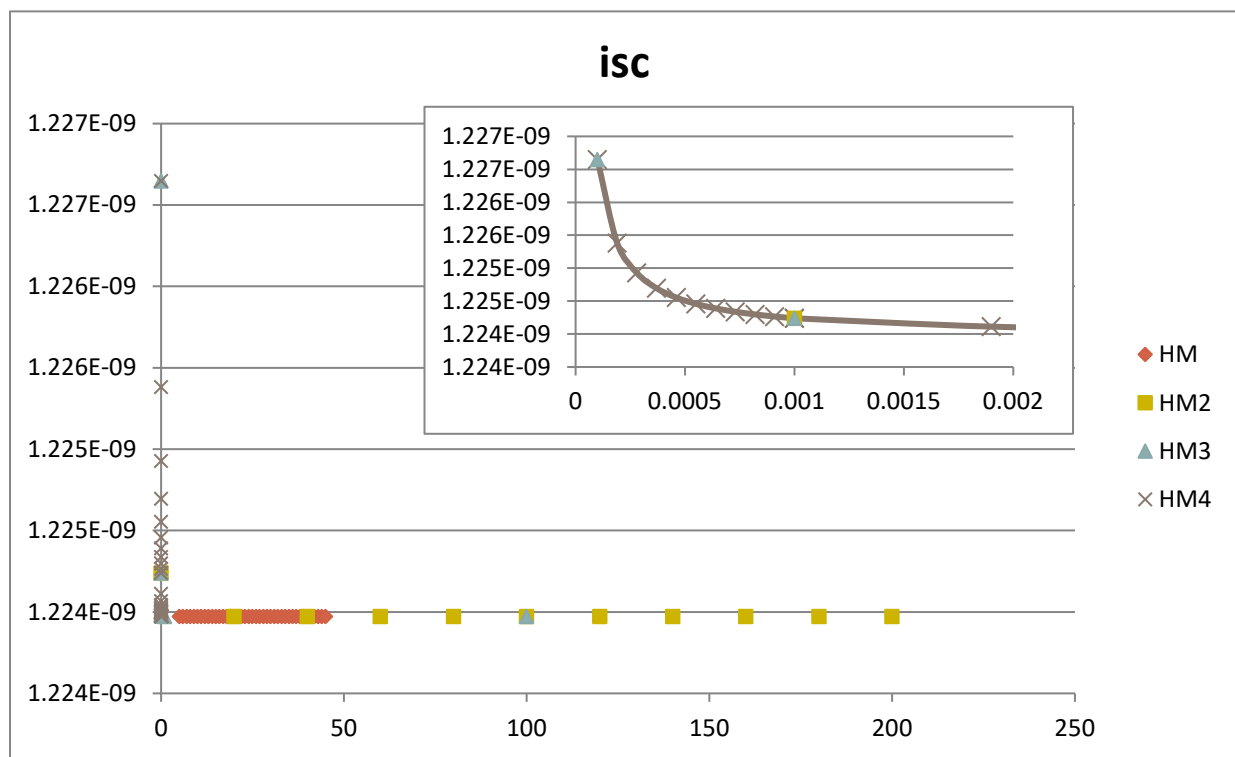
Figure 45: V_{OC} as a function of hole mobility
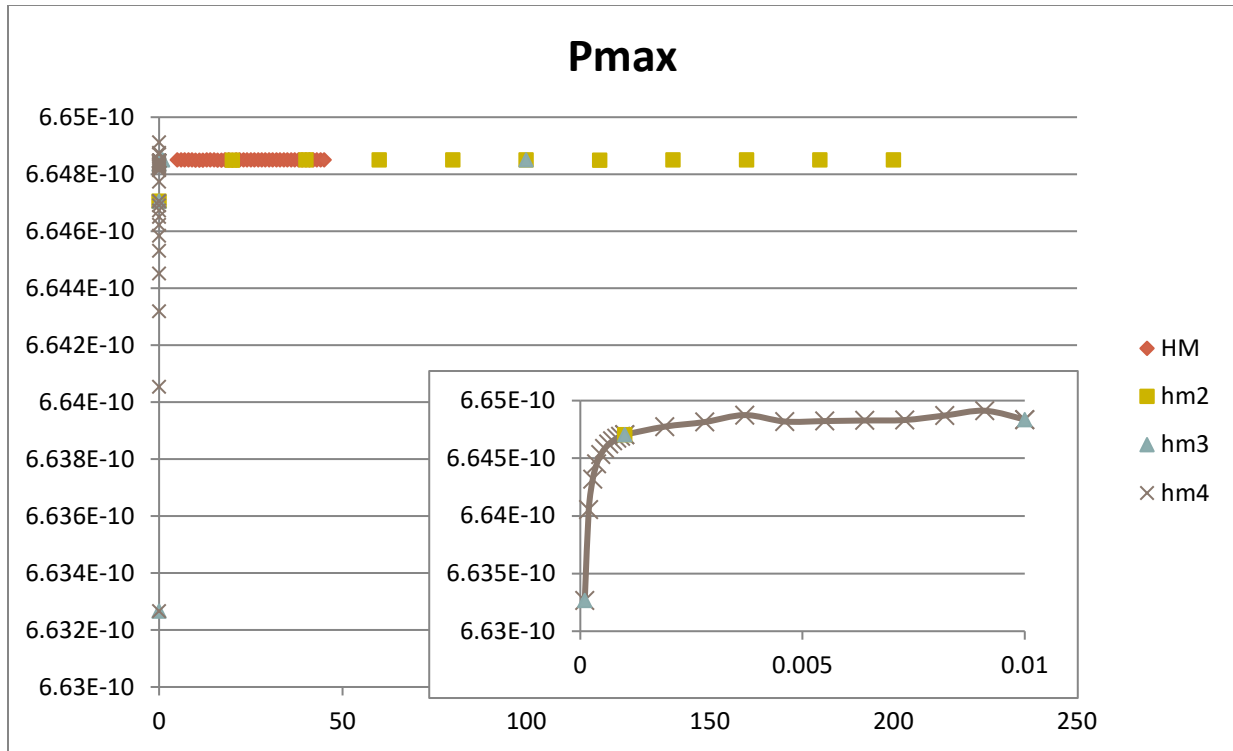

Figure 46: I_{sc} as a function of hole mobility

Figure 47: P$_{max}$ as a function of hole mobility
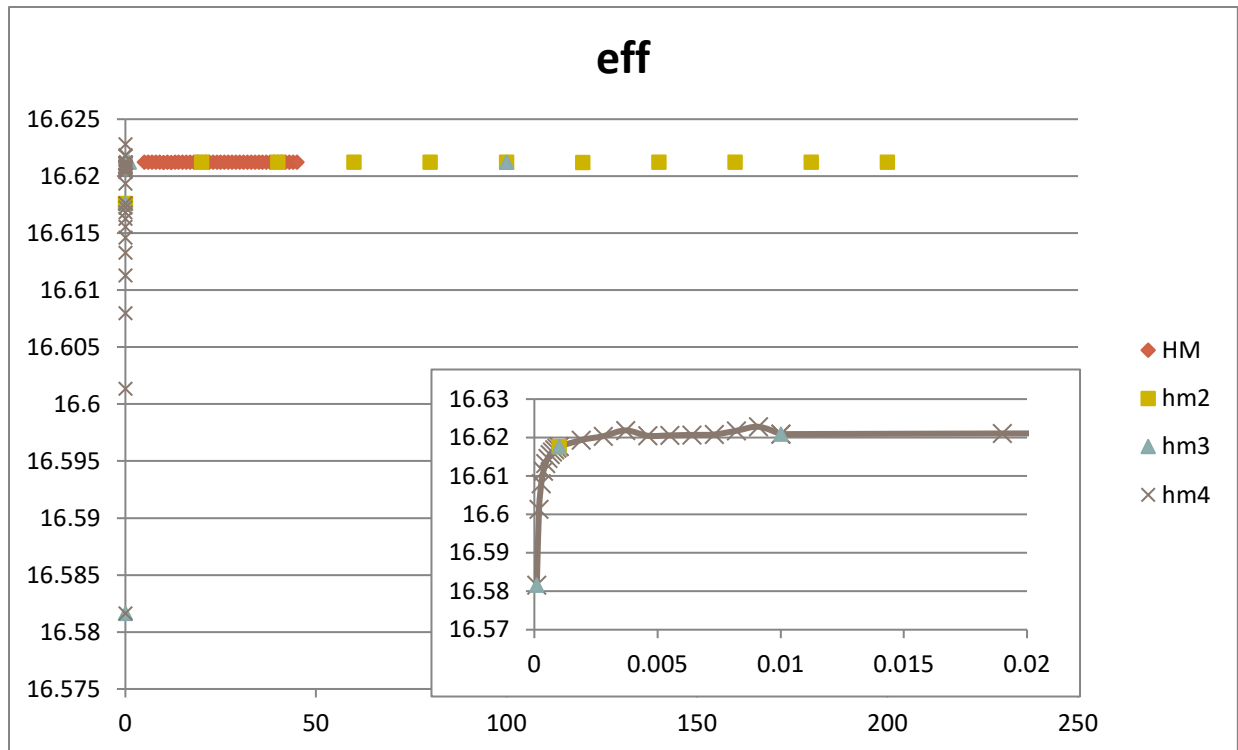
Figure 48: EFF as a function of hole mobility
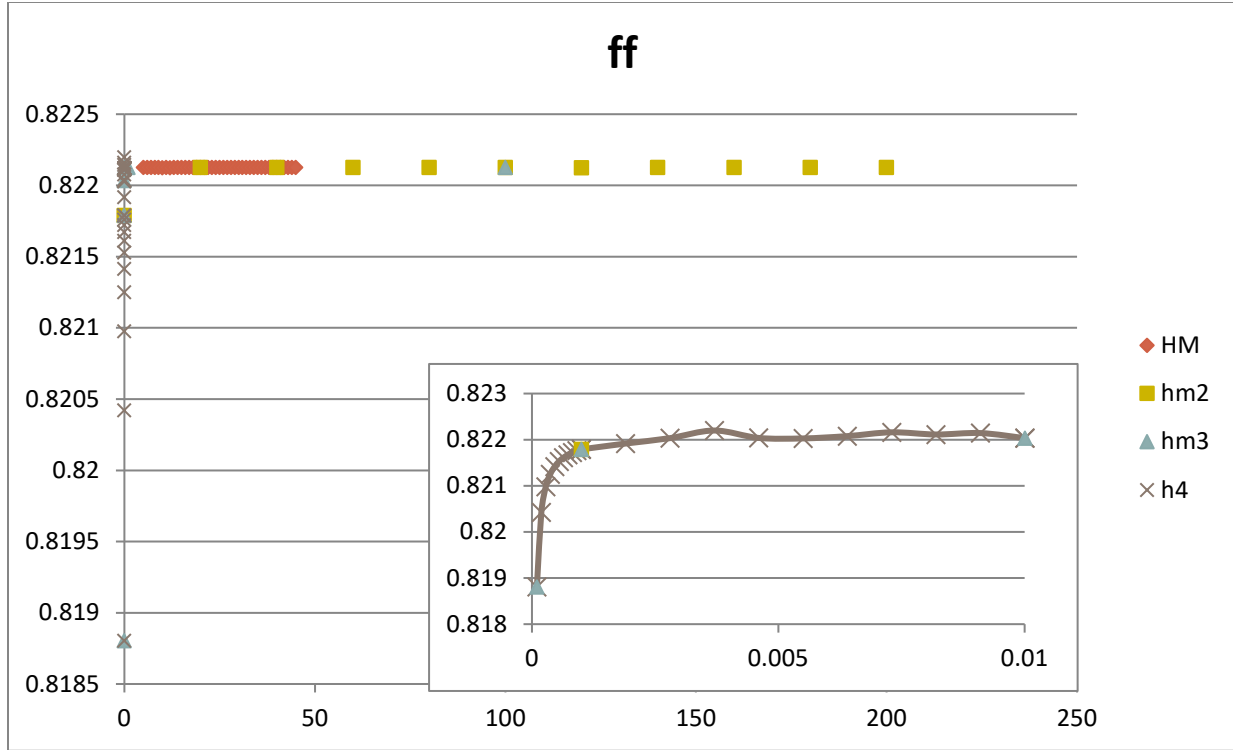
Figure 49: FF as a function of hole mobility

5.4.4 Hole life time

Figure 50 displays the effect of ole life time on open circuit voltage. It depicts a increasing exponential that levels off at 0.705 volts. Figure 51 displays the effects of hole life time on short circuit current, which shows an increasing exponential trend, the plateau of this trend has yet to be identified. Figures 52 and 53 display effects of hole life time on maximum power and the efficiency respectively, both show similar trends to the short circuit current. Figure 54 displays the effects of hole life time on the fill factor. The fill factor shows a different than the previous parameters. It has a large dampened oscillation that merges into an exponential which resembles that of the short circuit current. The transient region for all of the parameters is the same, which is a very small linear region.

Figure 50: V_{OC} as a function of hole life time
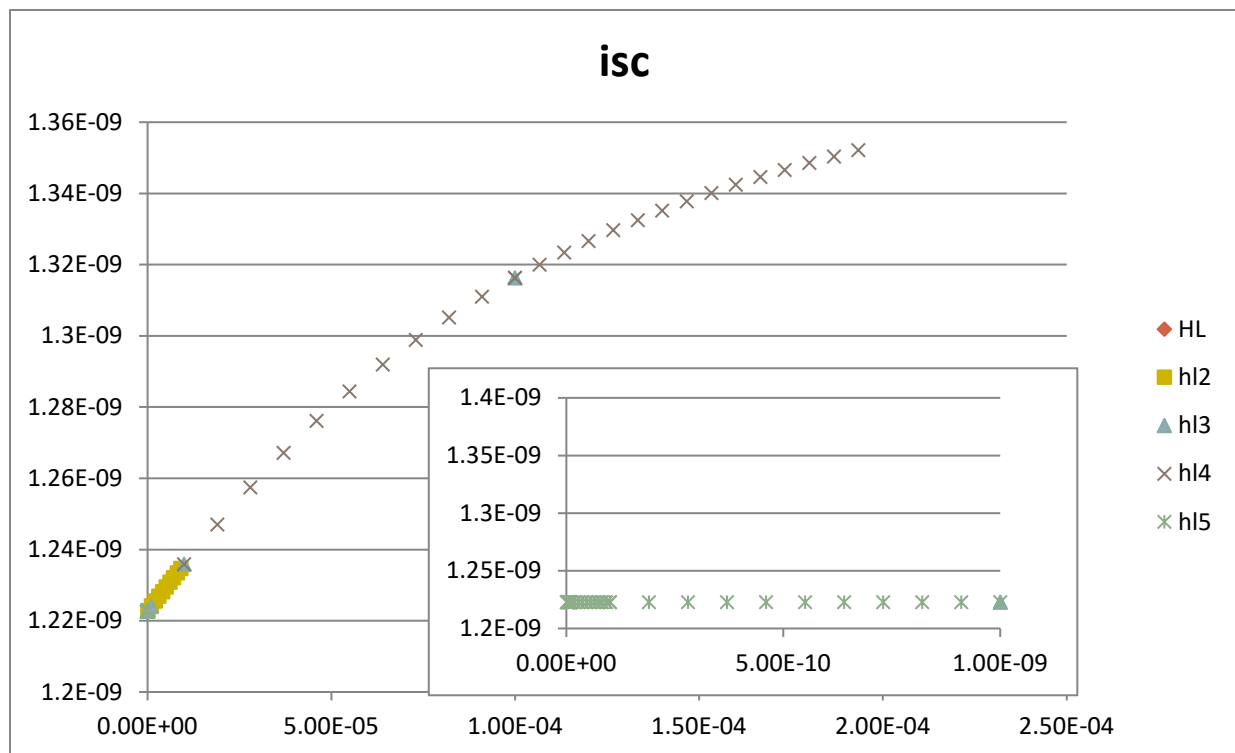
Figure 51: I_{SC} as a function of hole life time
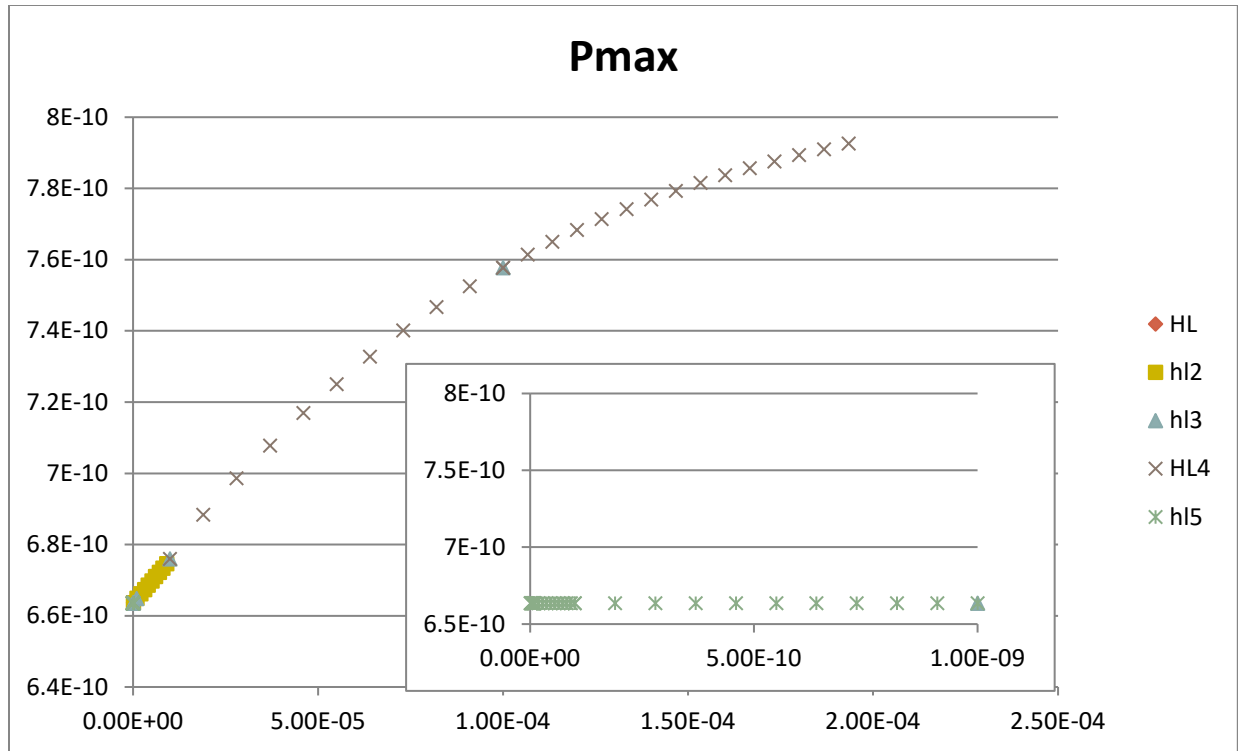
Figure 52: P_{MAX} as a function of hole life time
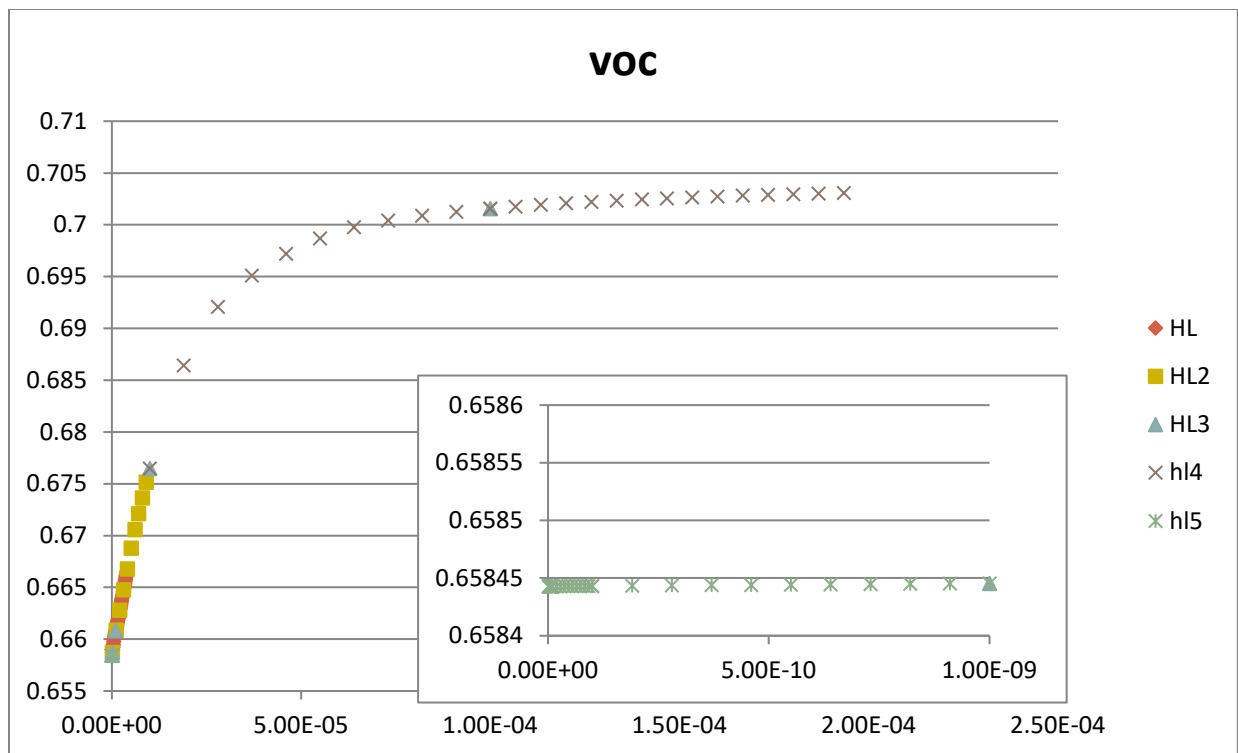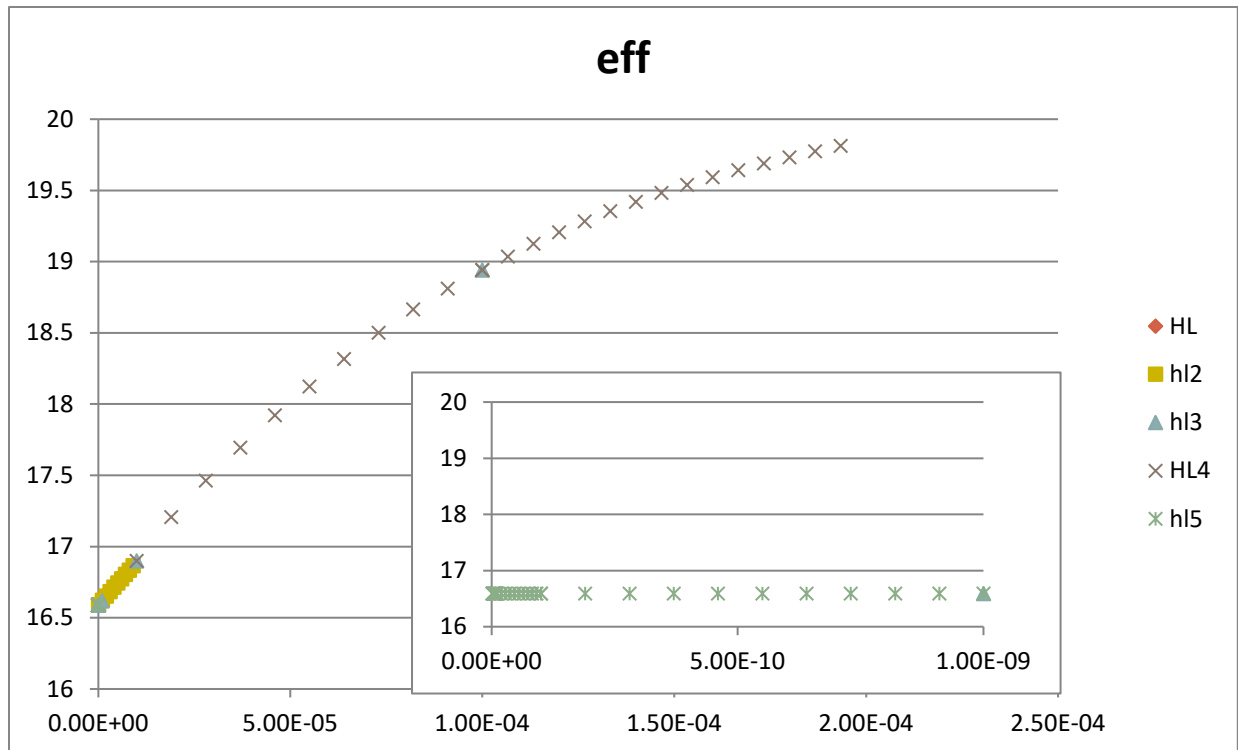

Figure 53: EFF as a function of hole life time
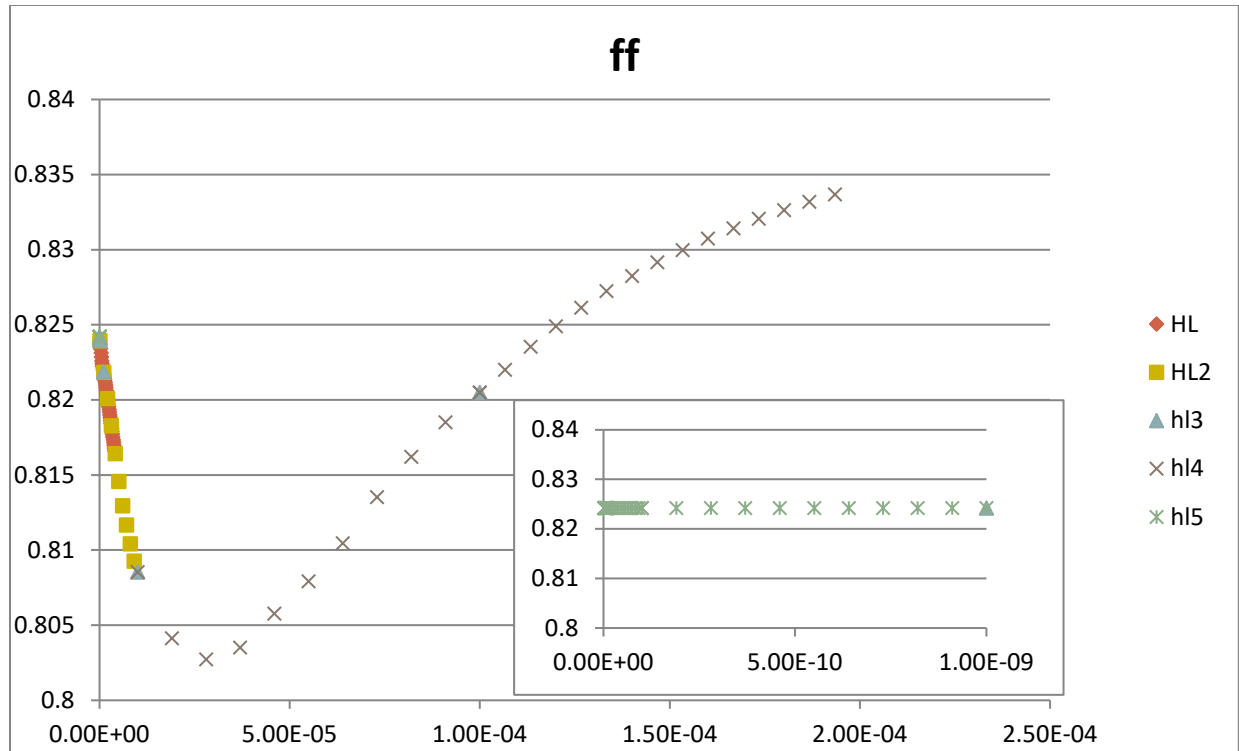
Figure 54: FF as a function of hole life time

5.4.5   Overall results of the study.

Figure 55 shows the region of the plots around the accepted values of CIGS material properties, which are listed in table 5, the data, can be compared to published results. I vertical line has been added to each plot to mark the location of the materials accepted value. Most of the results show the accepted value sitting in a relative flat region so if there is any variation there won't be any large changes to the V_{oc}, or the I_{sc}. There are two acceptations though. The electron life time sits on an increasing slope for the I_{sc}, and the hole life time site on a very slight increasing slope for the V_{oc}. Both of these trends agree with the published results.

Table 5: Accepted values for CIGS material properties

Electron Life time	2.00E-09	s
Hole Life time	1.00E-06	s
Electron Mobility	100	cm^2/Vs
Hole Mobility	25	cm^2/Vs
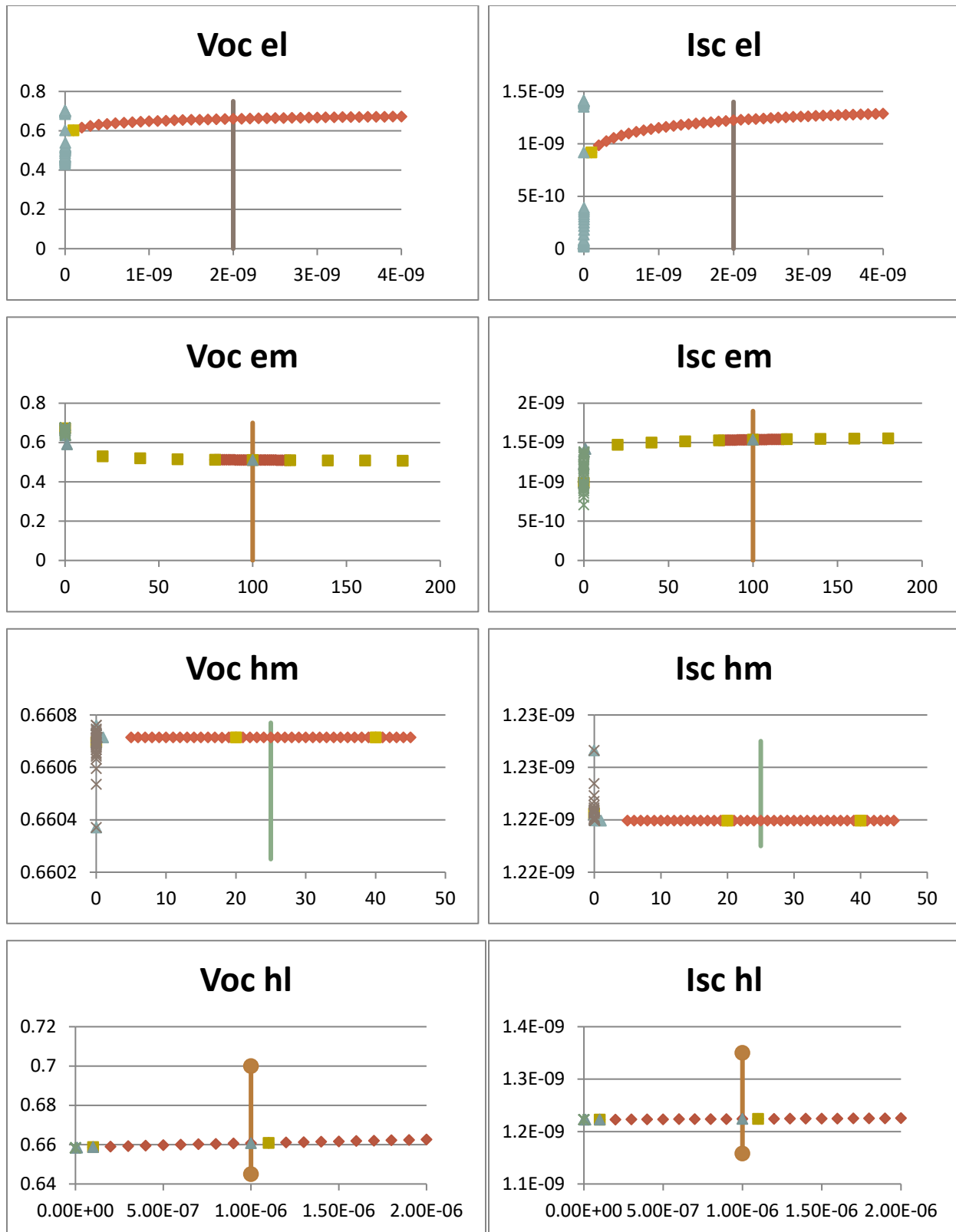
Figure 55: The effect of EM, EL, HM, and HL on V$_{OC}$, and I$_{SC}$ in the regions around the accepted values of the material properties

Comparing the two impactful plots, the Isc and the Voc to those from published results it can be seen how they relate. The plots from the parametric study, in figure 56, decrease in Isc, and Voc for electron life time and hole life time respectively. Looking at the J-V curves from Haque et al. [15] and Rahim et al [16] the same reduction in Isc and Voc can be seen for some form of change in electron and hole life time respectively
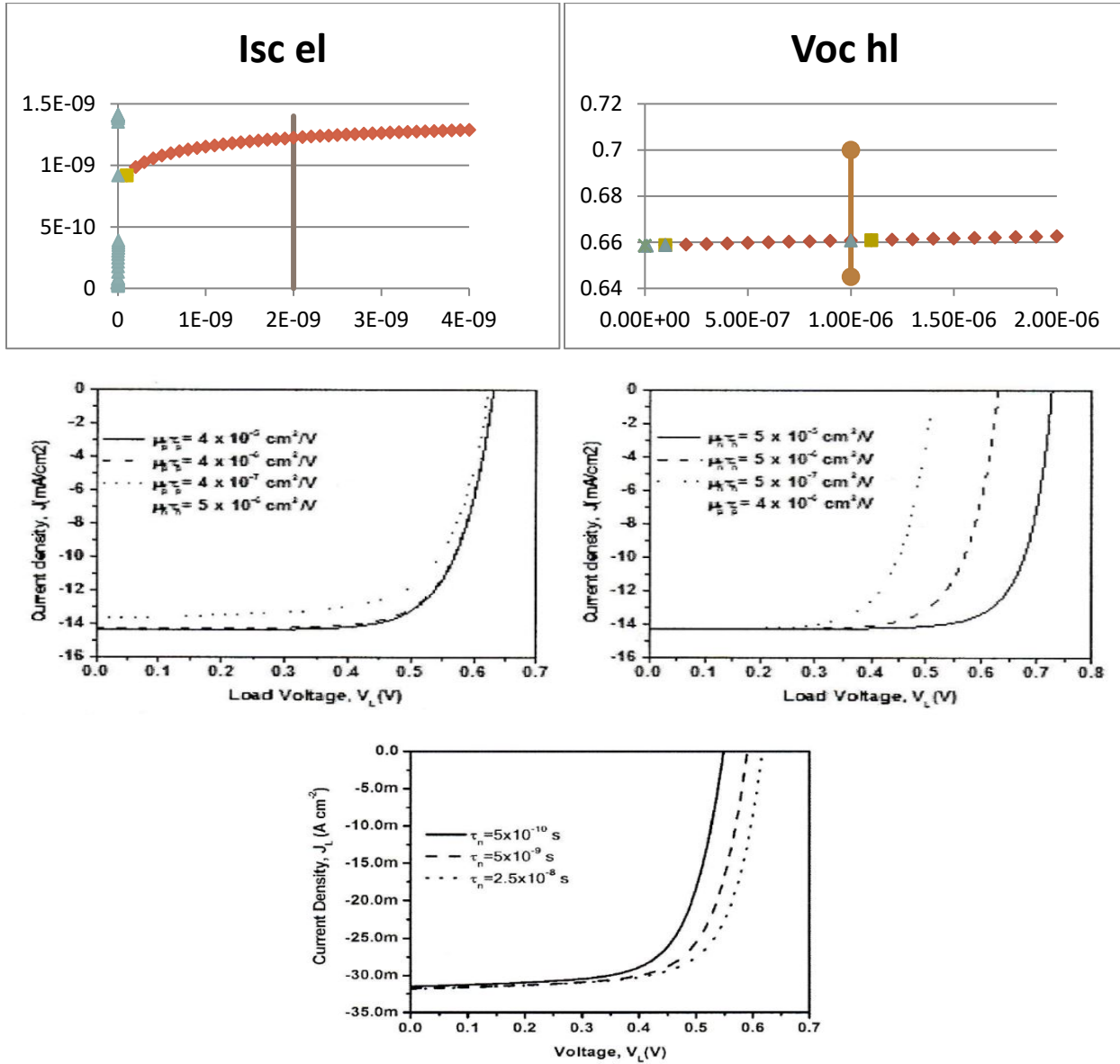
Figure 56: Top left: Change in Isc with respect to electron life time. Top right: Change in Voc with respect to hole life time. Middle left: Change in Isc with respect to the product of electron mobility and life time [15]. Middle right: Change in the Voc with respect to the product of hole mobility and life time [15]. Bottom: Change in the Voc with respect to electron life time [16].

6. CONCLUSION AND FUTURE WORK

6.1   Conclusion

In closing several trends relating to the generally effects of various applications of stress were found throughout this research. The stress can be categorized into two sets each with their own trend: Axial tensile stress, Bending/Rolling stress.

The axial tensile stress has shone a few distinct trends within the open circuit voltage and the short circuit current. For the V_{oc}, two trends were found. First is that open circuit voltage increases slightly with increasing stress. The other for rate of increase (the slope) increases with longer relaxation times. The short circuit current showed somewhat similar trends as the open circuit voltage. The two trends for the I_{sc}, were found to be that the short circuit current is larger with larger stress. The second is there seems to be a general increase in the Short circuit current up to a given threshold of stress. After that threshold the Short circuit current seems to decrease. The threshold stress varies depending on strain rate and relaxation time

The bending stress caused by holding the cell in fixed curves during operation did not did not have any noticeable effects to the open circuit voltage but for the short circuit current, maximum power, efficiency, and fill factor all showed a slight reduction in performance with the cell being bent in a concave position having a larger rate of decrease than the cell bent in a convex position. When taken in consideration with the rolling stress this trend continues up to a critical diameter. The critical diameter is between 2in and 1.75 in. Beyond the critical diameter the rate of performance reduction increases with the cell facing away from the dowel have much more rapid reduction than the cell facing the dowels. Both the bending and rolling results supports the concept that compressive stress is more damaging to the active layers than tensile stress.

Furthermore a set of theoretical trends have been established for V_{oc}, I_{sc}, P_{max}, EFF, and FF as a function of EM, EL, HM, and HM, independently from each other. These trends extend well into the regions that the materials would not naturally tend to have. This would allow for analysis of extreme degradation effects as well as a design tool for improving the performance of the solar cells by adjusting the EM, EL, HM, and HM parameters of the cells during fabrication.

6.2   Future Work

With tensile stress caused by bending the cell has less damaging effects than compressive bending stress, it is reasonable to assume that axle tensile stress also does not cause rapid degradation. This might be why it was difficult to find consistent results for the axle tensile experiments as there was not an effective method to precisely measure smaller fluctuations. To continue this particular set of experiments there needs to be a method of reducing the effects of relaxation on the cell. This can be done somewhat be keeping a constant strain rate and relaxation time for any further experiments. Another issue that can be solved is identifying the Young's modules and plastic deformation functions for each of the main layers of the solar cell. It was found that the Hanergy commercial solar cells have several layers that create a composite Young's Modules. If it is possible to obtain the Young's Modules for layers like the protective front surface coating, the back stainless steel, and the fabric-glue layers one would be able to calculate what portion of the load is being carried by the active layers. This can be done by assuming the entire solar cell is a set of parallel and series springs where the Young's Modules of each material is used as the spring constants. This would be a non-linear problem to solve and would most likely require a numerical analysis given that many of the materials used in these solar cells have highly plastic reactions to stress. The results from further experiments could also be processed with the matlab single diode curve fitting script to identify is axial tensile stress has any effect on Series and Shunt resistance as well as Dark current and Saturation current.

The base line values for electron mobility, electron life time, hole mobility, and hole life time, for the most part, fall within the stable plateau region of their effect on solar cell parameters, V_{oc}, I_{sc}, P_{max}, EFF, and FF. This means under normal operating conditions the variations of performance on these material properties might be negligible. They do need to be considered though if there is any damage as the damage to the crystalline structure of the active CIGS layer will change the mobility's and life times of the electrons and holes it is possible to fall into the regions where these properties do have great effect.

The bending and rolling experiments were done along different axis. The bending experiments were done with the bending moments along the vertical z-axis, while the bending moments from the rolling experiments were in the horizontal x-axis direction. A set of experiments for rolling and bending along different detections my e done to see there is directional lattice

dependency of the active layers. If this is known then manufacturers may be able to find ways to control the direction of the stress in the fabrication process to create more optimal solar cells.

Another thing to consider is reflective gains and losses when the cell is positioned in concave and convex positions while in operation. At this moment the intensity distribution equations do not take into account the reflective losses and gains of a cell. If the reflective gains and losses can be incorporated into the intensity distribution equation, it can be used to assist in improving the light source positioning and distribution reduce intensity deviations across the bent solar cells. With this adaptation to the intensity equations the results can be independent of intensity gradients and make the effects of the bending stress more prominent.

A base line of how electron mobility, electron life time, hole mobility, and hole life time effect solar cell parameters, such as open circuit voltage, short circuit current and fill factor, has been established. This base line can be used as a guide to find how stress affects these material properties. This can be done by identifying which set of EL, EM, HM, and HL creates a current density- voltage curve that matches an experimentally obtained curve. The key features to match between the simulated and experimental curves would the V_{oc}, I_{sc}, and FF. Matching the V_{oc}, and I_{sc} would allow one to identify the axis intercepts, while matching the FF would allow one to match the overall shape of simulated graph to the experimental graph. By matching each experimental current density- voltage curves in this way the trends for EM, EL, HM, and HL, can be found. This method can be used to find these types of trends for the Axial Tensile stress data, as well as the bending and rolling experimental data too.

REFERENCES

[1]   Tables for scenario projections," *World Energy Outlook World Energy Outlook 2019*, pp. 669–749, 2019.

[2]   R. Dieterich, E. Gies, G. Gustin, L. Gilpin, and L. Kaufman, "24-Hour Solar Energy: Molten Salt Makes It Possible, and Prices Are Falling Fast," *InsideClimate News*, 10-Apr-2019. [Online]. Available: https://insideclimatenews.org/news/16012018/csp-concentrated-solar-molten-salt-storage-24-hour-renewable-energy-crescent-dunes-nevada. [Accessed: 26-April-2020].

[3]   Jäger Klaus-Dieter, O. Isabella, A. H. M. Smets, Swaaij René A.C.M.M. van, and M. Zeman, *Solar energy: fundamentals, technology and systems*. Cambridge: UIT Cambridge, 2016.

[4]   J. Ramanujam and U. P. Singh, "Copper indium gallium selenide based solar cells – a review," *Energy & Environmental Science*, vol. 10, no. 6, pp. 1306–1319, 2017.

[5]   "Copper Indium Gallium Diselenide Solar Cells," *NREL.gov*. [Online]. Available: https://www.nrel.gov/pv/copper-indium-gallium-diselenide-solar-cells.html. [Accessed: 01-May-2020].

[6]   Y. Sun, S. Thompson and T. Nishida, Strain Effect in Semiconductors: Theory and Device Applications. New York, Springer Science+Business Media LLC, 2010.

[7]   K. Santhosh kumar, and R. Srinivasan, "Effect of Stress on the Performance of Silicon Solar Cell," International Journal of Innovative Research in Science, Engineering and Technology., vol.3, no.3, pp.725-730, Mar. 2014.

[8]   M. Salari and M. Joodaki, "Investigation of Electrical Characteristics Dependency of Roll-to-Roll Printed Solar Cells With Silver Electrodes on Mechanical Tensile Strain," *IEEE Transactions on Device and Materials Reliability*, vol. 19, no. 4, pp. 718–722, 2019.

[9]   E. Ungersboeck, S. Dhar, G. Karlowatz, H. Kosina, and S. Selberherr, "Physical modeling of electron mobility enhancement for arbitrarily strained silicon," J Comput Electron., vol. pp.55-58, Dec. 2007.

[10]   T.-K. Kang, "Evidence for Silicon Bandgap Narrowing in Uniaxially Strained MOSFETs Subjected to Tensile and Compressive Stress," *IEEE Electron Device Letters*, vol. 33, no. 6, pp. 770–772, 2012.

[11]   S. M. Lee, D. H. Yeon, B. C. Mohanty, and Y. S. Cho, "Tensile Stress-Dependent Fracture Behavior and Its Influences on Photovoltaic Characteristics in Flexible PbS/CdS Thin-Film Solar Cells," Acs Applied Materials & Interfaces, vol. 7, no. 8, pp. 4573-4578, Mar 2015

[12]   H. Kim, D. Xu, C. John, Y. Wu, "Modeling Thermo-mechanical stress of Flexible CIGS Solar Cell", IEEE JOURNAL OF PHOTOVOLTAICS, vol. 9, no. 2, pp 499-505, Mar 2019.

[13]   H. Kim, M. T. Tofail, and C. John, "The Effect of Interface Cracks on the Electrical Performance of Solar Cells," *Jom*, vol. 70, no. 4, pp. 473–478, 2018.

[14]   S. Wiedeman, "Cost and Reliability Improvement for CIGS-Based PV on Flexible Substrate," NREL report, 2011.

[15]   M. M. Haque, M. M. Rahman, and M. I. B. Chowdhury, "Current-voltage characteristics of CdS/CIGS thin film solar cells: An analytical approach," *2014 1st International Conference on Non Conventional Energy (ICONCE 2014)*, 2014.

[16]   A. B. Rahim, A. S. Hasan, P. Biswas, A. Ullah, and M. I. B. Chowdhury, "Analytical modeling of J-V characteristics of CIGS based thin film solar cell considering voltage and space dependent electric field in the absorber layer," *2015 International Conference on Advances in Electrical Engineering (ICAEE)*, 2015.

[17]   C. Nebel, H. Weller, and G. Bauer, "Electron mobility and lifetime in a-Si/sub 1-x/Ge/sub x/:H," *Conference Record of the Twentieth IEEE Photovoltaic Specialists Conference*, 1988.

[18]   "The Nobel Prize in Physics 1921," *NobelPrize.org*. [Online]. Available: https://www.nobelprize.org/prizes/physics/1921/summary/. [Accessed: 01-May-2020].

[19]   R. A. Serway, J. W. Jewett, and Peroomian Vahé, *Physics for scientists and engineers with modern physics*, 8th ed. Boston, MA: Brooks/Cole, Cengage Learning, 2012

[20]   J. R. Taylor, C. D. Zafiratos, and M. A. Dubson, *Modern physics for scientists and engineers*, 2nd ed. Upper Saddle River: Prentice Hall, 2004.

[21]   R. L. Liboff, *Introductory quantum mechanics*, 4th ed. San Francisco: Addison-Wesley, 2003.

[22]   C. Kittel and Krömer Herbert, *Thermal physics*, 2nd ed. New York, NY: Freeman, 1980.

[23]   C. Kittel, *Introduction to solid state physics*, 8th ed. New York: Wiley, 2005

[24]   D. J. Griffiths, *Introduction to electrodynamics*, 4th ed. Boston: Pearson, 2014.

[25] C. Liu, "Intro to Density-Gradient Theory for Semiconductor Device Simulation," *COMSOL Multiphysics*, 27-Nov-2019. [Online]. Available: https://www.comsol.com/blogs/intro-to-density-gradient-theory-for-semiconductor-device-simulation/. [Accessed: 17-April-2020].

[26] A. Shaik, " Electron and hole mobility," *Electron and hole mobility*. [Online]. Available: https://www.physics-and-radio-electronics.com/electronic-devices-and-circuits/semiconductor/electron-and-hole-mobility.html. [Accessed: 8-April-2020].

[27] *PVEducation*. [Online]. Available: https://www.pveducation.org/pvcdrom. [Accessed: 03-Nov-2018].

[28] W. D. Callister and D. G. Rethwisch, *Materials science and engineering: an introduction*. Hoboken, NJ: Wiley, 2014.

[29] "MATLAB," *MATLAB Documentation*. [Online]. Available: https://www.mathworks.com/help/matlab/index.html?s_tid=CRUX_lftnav. [Accessed: 20-Apr-2020].

[30] M. L. Gloeckler, A. R. Fahrenbruch, and J. undefined Sites, "Numerical Modeling of CIGS and CdTe solar cells: Setting the baseline. ," *3rd world conference on photovoltaic energy conversion*, pp. 491–494, May 2003